Bethe ansatz solution of triangular trimers on the triangular lattice

Alain Verberkmoes and Bernard Nienhuis
Instituut voor Theoretische Fysica, Universiteit van Amsterdam, Valckenierstraat 65, 1018 XE Amsterdam, The Netherlands
(Received 3 July 2000; published 24 May 2001)

Recently, a model consisting of triangular trimers covering the triangular lattice was introduced and its exact free energy given. In this paper we present the complete calculation leading to this exact result. The solution involves a coordinate Bethe ansatz with two kinds of particles. It is similar to that of the square-triangle random tiling model by Widom and Kalugin. The connection of the trimer model with related solvable models is discussed.

DOI: 10.1103/PhysRevE.63.066122 PACS number(s): 64.60.Cn, 05.50.+q, 05.70.−a

I. INTRODUCTION

The dimer problem is one of the classic models of statistical mechanics. A dimer in this context is a particle that occupies two neighboring sites of a lattice. In the dimer-monomer model, dimers and monomers (particles occupying one lattice site each) are placed on a lattice such that they cover all sites, without overlap. Equivalently the monomers can be viewed as empty sites; the lattice is then partly covered with dimers. This model was introduced to describe diatomic molecules adsorbed on a substrate [1]. Attempts have been made in vain to solve this model exactly, that is, to calculate its free energy. The special case that there are no empty sites (monomers) is now known as the dimer problem. There the dimers cover the lattice completely and without overlap. This model has been solved for planar lattices independently by Kasteleyn [2] and by Temperley and Fisher [3]. Their solution is based on the possibility to express the partition function of the model as a Pfaffian. For many planar lattices, the dimer problem can also be solved by means of the Bethe ansatz. On the honeycomb lattice, for example, it can be formulated as a five-vertex model. This is a special case of the six-vertex model whose Bethe ansatz solution is well known [4–11]. A review of the dimer problem is given in [12].

Inspired by the solvability of the dimer model, we consider lattice coverings by trimers. A trimer is a particle that occupies three lattice sites. We only consider triangular trimers, which live naturally on the triangular lattice. As in the dimer model, we require that these particles cover the lattice completely and without overlap. Thus every lattice site is covered by precisely one trimer. Figure 1 shows a typical configuration.

As will be shown in Sec. II B, the configurations of this model have a structure of domains separated by domain walls. The domains are hexagonal and the domain walls form a honeycomb network. Similar domain-wall structures are used to describe an incommensurate phase of a monolayer of a monoatomic gas adsorbed on a hexagonal substrate [13]. The entropy of such a network is largely due to the ''breathing'' of the cells: it is possible to enlarge a domain and simultaneously shrink its six neighbors or vice versa.

Hexagonal domain-wall structures also occur in the square-triangle random tiling model [14]. For that model a coordinate Bethe ansatz was found by Widom [15]. The resulting Bethe ansatz equations were solved analytically in the thermodynamic limit by Kalugin [16]. An exact solution of the trimer model was announced in [17]; in the present paper we describe its derivation. The solution is very similar to that for the square-triangle tiling, and we closely follow Kalugin's arguments. The outline of our calculation is as follows. A transfer matrix for the model is formulated. After the choice of a reference state two types of elementary excitations are found. They are closely related to the above-mentioned domain-wall structure of the model. In order to diagonalize the transfer matrix, a coordinate Bethe ansatz is set up in terms of the elementary excitations. The resulting semigrand canonical ensemble is discussed. In the thermodynamic limit the Bethe ansatz leads to a set of two coupled integral equations. These can be solved in a special case. From their solution the relevant physical quantities are computed. The results of the calculation are summarized in Sec. VI E. We then consider the entropy as function of the density of down trimers. The model undergoes two phase transitions in the density of down trimers.

Finally, we discuss the relation between the trimer model, the square-triangle random tiling model, and yet another solvable model with a hexagonal domain-wall structure.

II. PRELIMINARIES

A. Sublattices

Figure 2 shows a very regular configuration of the model in which the trimers are positioned on a sublattice of the triangular faces. There are six such sublattices, which we number 0, 1,..., 5 as indicated in the figure. Note that the even-numbered sublattices consist of the up triangles while

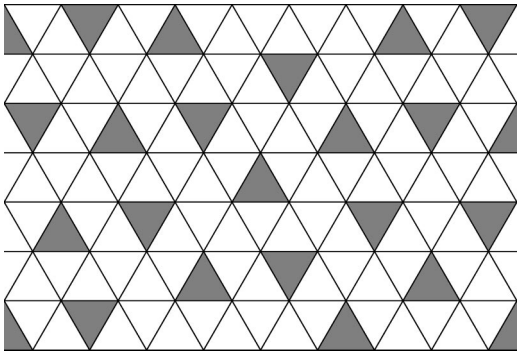

FIG. 1. A typical configuration of the trimer mode. Each lattice site belongs to precisely one trimer.

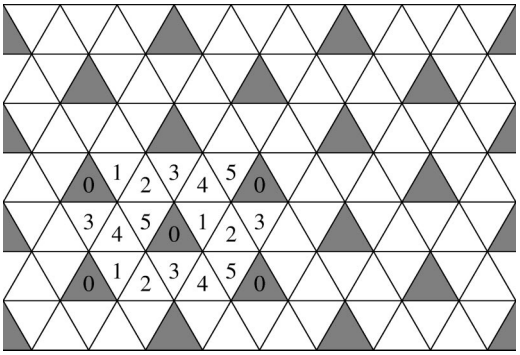

FIG. 2. A regular configuration in which the trimers occupy one sublattice of the faces. There are six such sublattices numbered 0, 1,..., 5.

the down triangles constitute the odd-numbered sublattices. For a given configuration, let N denote the total number of trimers and let N_i denote the number of trimers on sublattice i. We wish to compute the entropy per trimer as a function of the sublattice densities

$$\rho_0=\frac{N_0}{N}, \quad \rho_1=\frac{N_1}{N}, \quad \ldots, \quad \rho_5=\frac{N_5}{N}.$$

These densities satisfy the obvious linear constraint

$$\rho_0+\rho_1+\rho_2+\rho_3+\rho_4+\rho_5=1. \tag{1}$$

In Sec. II E it will be shown that when toroidal boundary conditions are imposed the densities also satisfy a quadratic constraint

$$\rho_0\rho_2+\rho_2\rho_4+\rho_4\rho_0=\rho_1\rho_5+\rho_3\rho_5+\rho_5\rho_1. \tag{2}$$

Hence, of the six sublattice densities only four are independent. In order to be able to set up a transfer matrix we pass to the grand canonical ensemble. The density of trimers on each sublattice i is controlled by a fugacity w_i or, equivalently, a chemical potential $\mu_i=\ln w_i$. After the transfer matrix has been diagonalized we shall Legendre transform back to the canonical ensemble.

B. Domains and walls

Occupying sublattice 0 completely while leaving the other five sublattices empty results in the configuration of the model shown in Fig. 2. This arrangement does not admit local changes. However, it is possible to flip a whole line of trimers. Such a line can be viewed as a wall separating two domains consisting of trimers on sublattice 0. These domain walls come in three types (orientations) corresponding to the three odd-numbered sublattices. When two walls of different types meet, a wall of a third type is formed. A trimer on sublattice 2 or 4 occurs when three domain walls of different types meet in a vertex shaped as a Y, but this does not happen at an inverted Y. Figure 3 shows examples of how the three types of domain walls can meet. In a general configuration the domain walls form a hexagonal network.

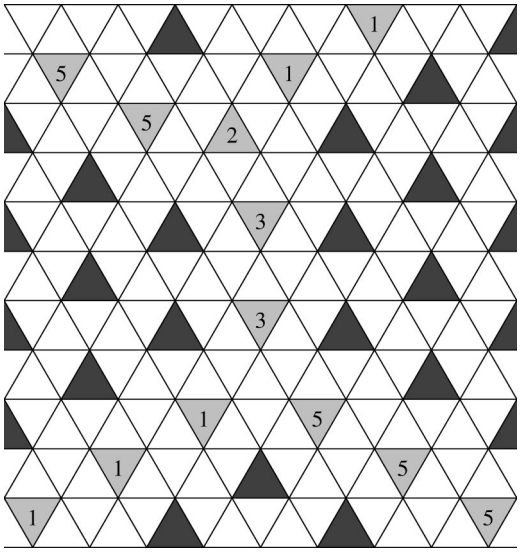

FIG. 3. The configuration from Fig. 2 admits line excitations. These domain walls can meet in Y's (top) and inverted Y's (bottom). The Y's are chiral; the mirror image of the Y shown here contains a trimer on sublattice 4 instead of 2. The inverted Y's are achiral. To guide the eye the trimers not on sublattice 0 are shaded lighter; the numbers indicate their sublattices.

C. Transfer matrix

In an allowed configuration of the model each lattice site belongs to precisely one trimer. This trimer sits either on one of the three lattice faces above the site or on one of the three faces below the site. Label the site with a ''spin'' $\uparrow$ or $\downarrow$ accordingly.

Consider a horizontal row of lattice sites and assume that the trimer configuration below that row is given. It determines the spins on that row. The sites occupied by a trimer below have a spin $\downarrow$ while those not occupied by such a trimer must carry a spin $\uparrow$. Now consider the next layer of lattice faces above this row. In order to decide what trimer configurations on this layer are possible, it is sufficient to know which sites are already covered. This is precisely the information encoded by the spins.

This shows that the model can be described in terms of a transfer matrix that connects two consecutive rows of spins. Let $\boldsymbol{\sigma}$ denote the spin configuration on the lower row and $\boldsymbol{\tau}$ the spin configurations on the upper row. Consider all the trimer arrangements (without overlaps) on the layer in between that are compatible with the spin configurations $\boldsymbol{\sigma}$ and $\boldsymbol{\tau}$. (Generally there is at most one such arrangement.) The sum of their Boltzmann weights is the transfer matrix element $T_{\tau\sigma}$.

D. Conserved quantities and elementary excitations

In the configuration obtained by fully occupying sublattice 0, each row of spins consists of repeating blocks $\uparrow\downarrow\uparrow$. Therefore we group the sites into blocks of three, as in Fig. 4. Number the blocks in a row from left to right.

Consider a trimer configuration on a layer of the lattice. Let L denote the number of blocks per row and let $n_0,n_1,\ldots,n_5$ denote the number of trimers in this layer on

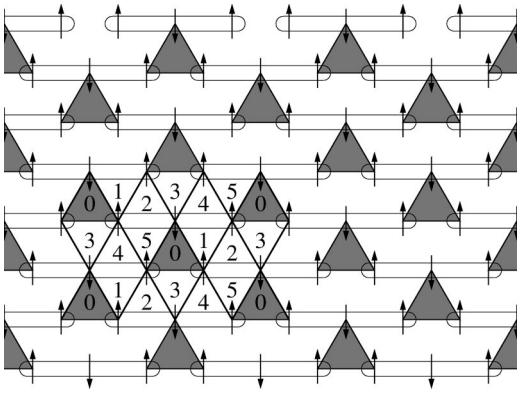

FIG. 4. Spins for the configuration from Fig. 2. For clarity, the edges of the triangular lattice have been largely omitted.

each sublattice. The horizontal and vertical lattice direction are viewed as ''space'' and ''time,'' respectively; the lower and upper row of the layer then are time-slices at times t and $t+1$. Counting the number of $\uparrow$ spins in the lower row and distinguishing by the position inside the block, gives

$$n^{(t)}_{\uparrow\bullet\,\bullet}=n_0+n_1+n_2.$$

$$n^{(t)}_{\bullet\uparrow\bullet}=n_2+n_3+n_4,$$

$$n^{(t)}_{\bullet\,\bullet\uparrow}=n_4+n_3+n_0.$$

From this, one gets

$$n^{(\tau)}_{\downarrow\bullet\,\bullet}+n^{(\tau)}_{\bullet\uparrow\bullet}=L-n_0-n_1+n_3+n_4, \tag{3}$$

$$n^{(\tau)}_{\bullet\,\bullet\downarrow}+n^{(\tau)}_{\bullet\uparrow\bullet}=L-n_0+n_2+n_3-n_5, \tag{4}$$

for $\tau=t$. The same can be done for the $\downarrow$ spins in the upper row. From this one gets that Eqs. (3) and (4) hold for $\tau=t+1$. Hence the quantities $n_{\downarrow\bullet\,\bullet}+n_{\bullet\uparrow\bullet}$ and $n_{\bullet\,\bullet\downarrow}+n_{\bullet\uparrow\bullet}$ are conserved between rows.

These conserved quantities are non-negative. The only row of spins for which both are zero consists entirely of blocks $\uparrow\downarrow\uparrow$. There is only one way to fit a layer of trimers above this row. Of course the row of spins above that layer consists again entirely of blocks $\uparrow\downarrow\uparrow$. This row state will be chosen as the ''empty'' or reference state for the Bethe ansatz in Sec. III.

A row of spins with $n_{\downarrow\bullet\,\bullet}+n_{\bullet\uparrow\bullet}=1$ and $n_{\bullet\,\bullet\downarrow}+n_{\bullet\uparrow\bullet}=0$ is obtained by replacing one block, say, at position x, in the reference state with $\downarrow\downarrow\uparrow$. There is only one possible configuration of trimers on the layer above, see Fig. 5. The row above consists of blocks $\uparrow\downarrow\uparrow$ except for one block $\downarrow\downarrow\uparrow$ at position $x-\frac{1}{2}$. Thus the transfer matrix has shifted the block

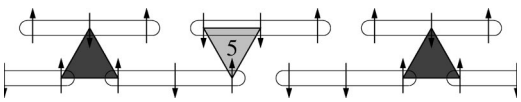

FIG. 5. There is only one way to fit trimers below a row consisting of one block $\downarrow\downarrow\uparrow$ amidst blocks $\uparrow\downarrow\uparrow$. It leads to another such row of spins below.

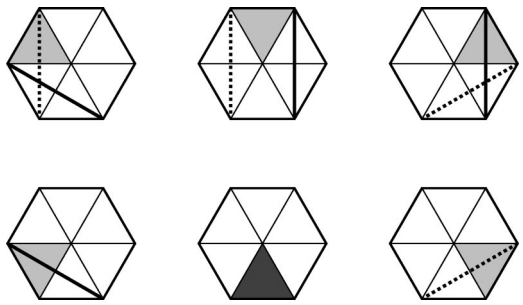

FIG. 6. Decompose the triangular lattice into hexagonal patches such that the lower middle triangle of each patch belongs to sublattice 0. The other triangles, in counterclockwise order, then belong to sublattices 1, 4, 3, 2, and 5. These patches can be decorated with the world lines of the L particles (solid) and R particles (dashed).

$\downarrow\downarrow\uparrow$ in the lower row half a step to the left in the upper row. This block is a left-moving elementary excitation of the reference state. It will be called an L particle. Similarly the block $\uparrow\downarrow\downarrow$ is an elementary right-moving excitation, or R particle. The conserved quantities $n_{\downarrow\bullet\,\bullet}+n_{\bullet\uparrow\bullet}$ and $n_{\bullet\,\bullet\downarrow}+n_{\bullet\uparrow\bullet}$ are the number n_{L} of L particles and the number n_{R} of R particles, respectively.

The particle content of the blocks $\uparrow\downarrow\uparrow$, $\downarrow\downarrow\uparrow$, and $\uparrow\downarrow\downarrow$ has now been determined. For each of the other five blocks both n_{L} and n_{R} are greater than zero. Therefore these blocks are combinations of the elementary excitations. They will be discussed in more detail in Secs. III C–III E.

We have found no other conserved quantities than n_{L} and n_{R} (except in the special case when $n_{\mathrm{L}}=0$ or $n_{\mathrm{R}}=0$).

E. World lines and quadratic constraint

Divide the lattice into hexagonal patches containing one face from each sublattice in such a way that the lower middle triangle of each patch belongs to sublattice 0. There are six trimer configurations possible on such a patch. Decorate each patch with solid and dotted lines according to this configuration as shown in Fig. 6. It is straightforward but tedious to verify that the decorations of the patches making up the lattice fit together such that the set of solid and dashed decorations run continuously from the bottom to the top of the lattice. It can also be checked that the crossings of these lines with the lattice rows correspond to the locations of the L particles (solid lines) and R particles (dashed lines). Hence these lines are the ''world lines'' of the L particles and R particles where the horizontal and vertical lattice direction are viewed as ''space'' and ''time,'' respectively.

Impose toroidal boundary conditions. We now derive the quadratic constraint (2) by the same method as that used for rectangle-triangle random tiling models in [18,19]. Cut the torus open along a horizontal row of sites so that the model is now on a cylinder. By stacking a number of copies of the configuration on top of each other, we can achieve that each world line winds around the cylinder an integer number of times. Let $2M$ be the number of rows in the configuration including these copies. In each row we can count the number of L particles and R particles [see Eqs. (3) and (4)],

$$n_{\mathrm{L}}=L-n_0-n_1+n_3+n_4, \tag{5}$$

$$n_R = L - n_0 + n_2 + n_3 - n_5. \quad (6)$$

Summing over the entire lattice yields

$$2Mn_L = 2LM - N_0 - N_1 + N_3 + N_4, \quad (7)$$

$$2Mn_R = 2LM - N_0 + N_2 + N_3 - N_5. \quad (8)$$

The total leftward movement of the L particles can be computed in two ways. On the one hand, it can be expressed in terms of the winding numbers of the L particle world lines. Since these world lines do not cross each other, they all have the same winding number W_L. On the other hand, leftward L particle movement is associated with trimers on sublattices 2 and 5, see Fig. 6. The same can be done for the total rightward movement of the R particles. Hence

$$n_L W_L L = \tfrac{1}{2}(N_2 + N_5), \quad (9)$$

$$n_R W_R L = \tfrac{1}{2}(N_1 + N_4). \quad (10)$$

The crossings of L-particle world lines and R-particle world lines can be counted in two ways. On the one hand, their number can be expressed in terms of the winding numbers. On the other hand, crossings occur precisely at trimers on sublattice 2 or 4. This yields

$$n_L n_R (W_L + W_R) = N_2 + N_4.$$

Substituting into the above equation, first Eqs. (9) and (10) and then Eqs. (7) and (8), then multiplying by $2LM$, using

$$2LM = N_0 + N_1 + N_2 + N_3 + N_4 + N_5$$

and dividing by N^2 yields the quadratic constraint (2).

III. BETHE ANSATZ

In this section we describe a Bethe ansatz (BA) that diagonalizes the transfer matrix. Since the particle numbers n_L and n_R are conserved, the transfer matrix is block diagonal in these quantities. We begin by considering the sector with $n_L = 0$ and $n_R = 0$ and then pass to sectors with higher particle numbers.

A. No particles

The only state in the sector $n_L = 0$, $n_R = 0$ is the reference state that consists entirely of blocks $\uparrow\downarrow\uparrow$, so this sector is one dimensional. Therefore the transfer matrix acting on this sector is trivially diagonal. The layer between two consecutive rows in the reference state consists of L trimers on sublattice 0, so its Boltzmann weight is w_0^L. It is the eigenvalue of the transfer matrix in this sector. For convenience we define the ''reduced'' transfer matrix $\tilde{T}$ to be the transfer matrix T divided by w_0^L.

B. One L particle

Consider a row of spins containing a single L particle ($\downarrow\downarrow\uparrow$) at position x. The transfer matrix has shifted this particle from position $x + \frac{1}{2}$ in the row below half a step to the left, see Fig. 5. The layer between the two rows contains $L - 1$ trimers on sublattice 0 and one trimer on sublattice 5. Hence the action of the (reduced) transfer matrix on the ''wave function'' is given by

$$(\tilde{T}\psi)(\downarrow\downarrow\uparrow x) = \frac{w_5}{w_0}\psi(\downarrow\downarrow\uparrow x + \tfrac{1}{2}).$$

(We use $\downarrow\downarrow\uparrow x$ as notation for the row configuration that has a block $\downarrow\downarrow\uparrow$ at position x and blocks $\uparrow\downarrow\uparrow$ at the other positions.) The solution of the eigenvalue problem $\tilde{T}\psi = \tilde{\Lambda}\psi$ is

$$\psi(\downarrow\downarrow\uparrow x) = A_u u^x,$$

where A_u is some constant and

$$\tilde{\Lambda} = \frac{w_5}{w_0} u^{1/2}.$$

C. One L particle and one R particle

Consider a row of spins containing an L particle ($\downarrow\downarrow\uparrow$) at position x and an R particle ($\uparrow\downarrow\downarrow$) at position y with $x < y$. If the particles are apart, this situation was formed by shifting the L particle to the left and the R particle to the right,

$$(\tilde{T}\psi)(\downarrow\downarrow\uparrow x, \uparrow\downarrow\downarrow y) = \frac{w_5 w_1}{w_0^2}\psi(\downarrow\downarrow\uparrow x + \tfrac{1}{2}, \uparrow\downarrow\downarrow y - \tfrac{1}{2}) \quad \text{if } y - x > 1. \quad (11)$$

[We write the arguments of ψ in order of increasing position; for example, the notation in the left-hand side (LHS) of Eq. (11) implies that $x < y$.] If, however, the particles are next to each other, the situation was formed from a ''bound state'' ($\downarrow\downarrow\downarrow$), see Fig. 3 (top),

$$(\tilde{T}\psi)(\downarrow\downarrow\uparrow z - \tfrac{1}{2}, \uparrow\downarrow\downarrow z + \tfrac{1}{2}) = \frac{w_5 w_1}{w_0^2}\psi(\downarrow\downarrow\downarrow z). \quad (12)$$

This bound state was formed from another type of bound state ($\uparrow\uparrow\uparrow$),

$$(\tilde{T}\psi)(\downarrow\downarrow\downarrow z) = \frac{w_4 w_1}{w_0}\psi(\uparrow\uparrow\uparrow z - \tfrac{1}{2}) + \frac{w_5 w_2}{w_0}\psi(\uparrow\uparrow\uparrow z + \tfrac{1}{2}). \quad (13)$$

The two terms correspond to two chiral configurations, one of which is depicted in Fig. 3. The latter bound state ($\uparrow\uparrow\uparrow$) was formed from an R particle and an L particle in adjacent blocks, the R particle sitting to the left of the L particle,

$$(\tilde{T}\psi)(\uparrow\uparrow\uparrow z) = \frac{1}{w_0}\psi(\uparrow\downarrow\downarrow z - \tfrac{1}{2}, \downarrow\downarrow\uparrow z + \tfrac{1}{2}). \quad (14)$$

This configuration may have arisen from the same bound state again. The alternation of this bound state and the situation where the R particle and L particle are next to each other ($\uparrow\downarrow\downarrow$ $\downarrow\downarrow\uparrow$) corresponds to the vertical domain wall in Fig. 3. The configuration where the particles are next to each other may also have arisen from a situation where the par-

ticles were two steps apart, by shifting the R particle half a step to the right and the L particle half a step to the left, see Fig. 3 (bottom),

$$(\tilde{T}\psi)(\uparrow\downarrow\downarrow z-\tfrac{1}{2},\downarrow\downarrow\uparrow z+\tfrac{1}{2})=w_3\psi(\uparrow\uparrow\uparrow z)+\frac{w_1w_5}{w_0^2}\psi(\uparrow\downarrow\downarrow z-1,\downarrow\downarrow\uparrow z+1). \tag{15}$$

Finally, a configuration where the particles are apart was formed by shifting the R particle half a step to the right and the L particle half a step to the left,

$$(\tilde{T}\psi)(\uparrow\downarrow\downarrow y,\downarrow\downarrow\uparrow x)=\frac{w_1w_5}{w_0^2}\psi(\uparrow\downarrow\downarrow y-\tfrac{1}{2},\downarrow\downarrow\uparrow x+\tfrac{1}{2}) \quad \text{if } x-y>1. \tag{16}$$

We want to solve the eigenvalue equation $\tilde{T}\psi=\tilde{\Lambda}\psi$ for Eqs. (11)–(16). The eigenvalue equation for Eqs. (11) and (12) is satisfied by

$$\psi(\downarrow\downarrow\uparrow x,\uparrow\downarrow\downarrow y)=A_{uv}u^xv^y,$$

$$\psi(\downarrow\downarrow\downarrow z)=A_{uv}u^zv^z$$

with eigenvalue

$$\tilde{\Lambda}=\frac{w_5}{w_0}u^{1/2}\frac{w_1}{w_0}v^{-1/2}.$$

Similarly the eigenvalue equation for Eqs. (14), (15), and (16), with the same $\tilde{\Lambda}$, is satisfied by

$$\psi(\uparrow\downarrow\downarrow y,\downarrow\downarrow\uparrow x)=A_{vu}v^yu^x \quad \text{if } x-y>1,$$

$$\psi(\uparrow\downarrow\downarrow z-\tfrac{1}{2},\downarrow\downarrow\uparrow z+\tfrac{1}{2})=B_{vu}A_{vu}v^{z-1/2}u^{z+1/2},$$

$$\psi(\uparrow\uparrow\uparrow z)=DB_{vu}A_{vu}v^zu^z,$$

where

$$B_{vu}=\left(1-\frac{w_0^3w_3}{w_1^2w_5^2}u^{-1}v\right)^{-1}, \tag{17}$$

$$D=\frac{w_0}{w_1w_5}. \tag{18}$$

The eigenvalue equation for Eq. (13) is satisfied too if

$$\frac{A_{uv}}{A_{vu}}=S_{uv},$$

where

$$S_{uv}=\frac{w_0^2}{w_1w_5}\left(\frac{w_4}{w_5}u^{-1}+\frac{w_2}{w_1}v\right)\left(1-\frac{w_0^3w_3}{w_1^2w_5^2}u^{-1}v\right)^{-1}. \tag{19}$$

The above analysis suggests to interpret the bound state $\downarrow\downarrow\downarrow$ as LR (in that order) and the bound state $\uparrow\uparrow\uparrow$ as RL. The eigenfunction is then written

$$\psi(\mathrm{L}x,\mathrm{R}y)=A_{uv}u^xv^y,$$

$$\psi(\mathrm{R}y,\mathrm{L}x)=\begin{cases} A_{vu}v^yu^x & \text{if } x-y\geqslant 2 \\ B_{vu}A_{vu}v^yu^x & \text{if } x-y=1 \\ DB_{vu}A_{vu}v^yu^x & \text{if } x-y=0. \end{cases}$$

D. Two L particles and one R particle

A similar but more tedious analysis can be carried out for the sector with two L particles and one R particle. There is a new bound state $(\downarrow\uparrow\uparrow)$ that can be interpreted as LRL. A solution of the eigenvalue problem $\tilde{T}\psi=\tilde{\Lambda}\psi$ is given by

$$\psi(\mathrm{L}x_1,\mathrm{L}x_2,\mathrm{R}y)=\sum_\pi A_{u_{\pi(1)}u_{\pi(2)}v}u_{\pi(1)}^{x_1}u_{\pi(2)}^{x_2}v^y,$$

$$\psi(\mathrm{L}x_1,\mathrm{R}y,\mathrm{L}x_2)=\begin{cases} \sum_\pi A_{u_{\pi(1)}vu_{\pi(2)}}u_{\pi(1)}^{x_1}v^yu_{\pi(2)}^{x_2} & \text{if } x_2-y\geqslant 2 \\ \sum_\pi B_{vu_{\pi(2)}}A_{u_{\pi(1)}vu_{\pi(2)}}u_{\pi(1)}^{x_1}v^yu_{\pi(2)}^{x_2} & \text{if } x_2-y=1 \\ \sum_\pi DB_{vu_{\pi(2)}}A_{u_{\pi(1)}vu_{\pi(2)}}u_{\pi(1)}^{x_1}v^yu_{\pi(2)}^{x_2} & \text{if } x_2-y=0, \end{cases}$$

$$\psi(\mathrm{R}y,\mathrm{L}x_1,\mathrm{L}x_2)=\begin{cases} \sum_\pi A_{vu_{\pi(1)}u_{\pi(2)}}v^yu_{\pi(1)}^{x_1}u_{\pi(2)}^{x_2} & \text{if } x_1-y\geqslant 2 \\ \sum_\pi B_{vu_{\pi(1)}}A_{vu_{\pi(1)}u_{\pi(2)}}v^yu_{\pi(1)}^{x_1}u_{\pi(2)}^{x_2} & \text{if } x_1-y=1 \\ \sum_\pi DB_{vu_{\pi(1)}}A_{vu_{\pi(1)}u_{\pi(2)}}v^yu_{\pi(1)}^{x_1}u_{\pi(2)}^{x_2} & \text{if } x_1-y=0, \end{cases}$$

where π runs through the permutations of {1,2}. The amplitudes must satisfy

$$\frac{A_{u_i u_{i'} v}}{A_{u_{i'} u_i v}} = \frac{A_{v u_i u_{i'}}}{A_{v u_{i'} u_i}} = -1 \quad (i \neq i'), \tag{20}$$

$$\frac{A_{u_i v u_{i'}}}{A_{v u_i u_{i'}}} = \frac{A_{u_{i'} u_i v}}{A_{u_{i'} v u_i}} = S_{u_i v} \quad (i \neq i'), \tag{21}$$

with $S_{u_i v}$ given by Eq. (19). Note that the amplitude ratios in Eq. (20) do not depend on v and that the amplitude ratios in Eq. (21) do not depend on $u_{i'}$. The eigenvalue is given by

$$\tilde{\Lambda} = \frac{w_5}{w_0} u_1^{1/2} \frac{w_5}{w_0} u_2^{1/2} \frac{w_1}{w_0} v^{-1/2}.$$

E. Arbitrary particle numbers

With two L particles and two R particles, there is a new bound state ($\downarrow\uparrow\downarrow$) that can be interpreted as LRLR. This completes the list of possible blocks and their interpretation in terms of particles, see Table I.

The solution given above of the eigenvalue problem $\tilde{T}\psi = \tilde{\Lambda}\psi$ for two L particles and one R particle generalizes to the higher sectors. Before describing this generalization we introduce a notational convention. The index i, running from 1 to n_{L}, will be used to number L-particle positions and Bethe-ansatz variables. The index j, between 1 and n_{R}, will refer to R particles. Now consider a succession of L particles with coordinates $x_1 \leqslant x_2 \leqslant \cdots \leqslant x_{n_{\mathrm{L}}}$ and R particles with coordinates $y_1 \leqslant y_2 \leqslant \cdots \leqslant y_{n_{\mathrm{R}}}$. (Note that $x_i = x_{i+1}$ can arise only from a block LRL or LRLR, so $x_i = y_j = x_{i+1}$ for some y_j.) The value of the wave function is given by

$$\psi(\text{particle sequence}) = \sum_{\pi} \sum_{\sigma} \prod (D \text{ and } B \ldots) A \ldots \prod_{i=1}^{n_{\mathrm{L}}} u_{\pi(i)}^{x_i} \prod_{j=1}^{n_{\mathrm{R}}} v_{\sigma(j)}^{y_j}, \tag{22}$$

where π and σ run through all permutations of {1, 2,..., n_{L}} and {1, 2,..., n_{R}}, respectively. We shall now describe the factors in the right-hand side (RHS) of Eq. (22). For each segment $\mathrm{R}\, y_j, \mathrm{L}\, x_i$ in the particle sequence with $x_i - y_j = 1$, there is a factor $B_{v_{\sigma(j)} u_{\pi(i)}}$. For each such segment with $x_i - y_j = 0$, there is a factor $DB_{v_{\sigma(j)} u_{\pi(i)}}$. The amplitude $A \ldots$ depends on the sequence of the variables u and v corresponding to the sequence of L particles and R particles. The u's are in the order $u_{\pi(1)}, u_{\pi(2)}, \ldots, u_{\pi(n_{\mathrm{L}})}$ and the v's are in the order $v_{\sigma(1)}, v_{\sigma(2)}, \ldots, v_{\sigma(n_{\mathrm{R}})}$, but the two sequences interlace. The amplitudes $A \ldots$ are defined up to an overall factor by the conditions

$$\frac{A_{\ldots u_i u_{i'} \ldots}}{A_{\ldots u_{i'} u_i \ldots}} = -1 \quad (i \neq i'),$$

$$\frac{A_{\ldots v_j v_{j'} \ldots}}{A_{\ldots v_{j'} v_j \ldots}} = -1 \quad (j \neq j'),$$

$$\frac{A_{\ldots u_i v_j \ldots}}{A_{\ldots v_j u_i \ldots}} = S_{u_i v_j}$$

with $S_{u_i v_j}$ given by Eq. (19). Finally comes the product of all the $u_{\pi(i)}^{x_i}$ and $v_{\sigma(j)}^{y_j}$. The eigenvalue for the eigenfunction ψ is given by

$$\tilde{\Lambda} = \prod_{i=1}^{n_{\mathrm{L}}} \frac{w_5}{w_0} u_i^{1/2} \prod_{j=1}^{n_{\mathrm{R}}} \frac{w_1}{w_0} v_j^{-1/2}.$$

We have no rigorous proof that the above solution is correct for all sectors, but using computer algebra we have verified it for $n_{\mathrm{L}} + n_{\mathrm{R}} \leqslant 5$.

It should be noted that the formulation of the solution depends on the particle interpretation of the three-spin blocks. The particle content of each three-spin block is determined by $n_{\mathrm{L}} = n_{\downarrow\bullet\bullet} + n_{\bullet\uparrow\bullet}$ and $n_{\mathrm{R}} = n_{\downarrow\bullet\bullet} + n_{\bullet\uparrow\bullet}$, but the order of the particles within a block can be chosen. For example, we could interpret $\downarrow\uparrow\uparrow$ as LLR, LRL, or RLL. The choices in Table I lead to a simple description of the eigenfunctions; each factor D or B depends only on two successive particles. Other choices than those in Table I would make the formulation of the eigenfunctions more cumbersome; there would be more factors than just D and B, and some would depend on nonsuccessive particles.

TABLE I. The three-spin blocks.

Spins	Particles
$\uparrow\downarrow\uparrow$	None
$\downarrow\downarrow\uparrow$	L
$\uparrow\downarrow\downarrow$	R
$\downarrow\downarrow\downarrow$	LR
$\uparrow\uparrow\uparrow$	RL
$\downarrow\uparrow\uparrow$	LRL
$\uparrow\uparrow\downarrow$	RLR
$\downarrow\uparrow\downarrow$	LRLR

F. Bethe ansatz equations

The eigenfunction ψ given by Eq. (22) satisfies periodic boundary conditions if the Bethe ansatz equations (BAE's) hold,

$$u_i^L = (-1)^{n_{\mathrm{L}}-1} \prod_{j=1}^{n_{\mathrm{R}}} S_{u_i v_j}, \tag{23}$$

$$v_j^L = (-1)^{n_{\mathrm{R}}-1} \prod_{i=1}^{n_{\mathrm{L}}} S_{u_i v_j}^{-1}. \tag{24}$$

Note that although the description of an eigenfunction in terms of u's and v's involves factors (17) and (18), the BAE's only contain factors (19).

Upon substitution of

$$u=\left(\frac{w_0^3 w_3 w_4}{w_1 w_2 w_5^3}\right)^{1/2}\xi \quad \text{and} \quad v=-\left(\frac{w_1^3 w_4 w_5}{w_0^3 w_2 w_3}\right)^{1/2}\eta^{-1} \tag{25}$$

the BAE's (23) and (24) become

$$\left(\frac{w_0^3 w_3 w_4}{w_1 w_2 w_5^3}\right)^{L/2}\left(\frac{w_1 w_3 w_5}{w_0 w_2 w_4}\right)^{n_R/2}\xi_i^L = (-1)^{n_L+n_R-1}\prod_{j=1}^{n_R}\eta_j^{-1}\frac{\xi_i-\eta_j}{\xi_i+\eta_j^{-1}}, \tag{26}$$

$$\left(\frac{w_0^3 w_2 w_3}{w_1^3 w_4 w_5}\right)^{L/2}\left(\frac{w_1 w_3 w_5}{w_0 w_2 w_4}\right)^{n_L/2}\eta_j^L = (-1)^{L+n_R-1}\prod_{i=1}^{n_L}\xi_i^{-1}\frac{\eta_j-\xi_i}{\eta_j+\xi_i^{-1}}. \tag{27}$$

These equations can be considered the key result in the exact solution of the model. They determine the possible values for ξ and η. These in turn determine the eigenvalues and the eigenfunctions of the transfer matrix,

$$\Lambda = w_0^L\left(\frac{w_3 w_4 w_5}{w_0 w_1 w_2}\right)^{n_L/4}\left(\frac{w_1 w_2 w_3}{w_0 w_4 w_5}\right)^{n_R/4}\times\left[\prod_{i=1}^{n_L}\xi_i\prod_{j=1}^{n_R}(-\eta_j)\right]^{1/2}, \tag{28}$$

where we have reintroduced the factor w_0^L that was omitted as of Sec. III A.

As a check on the Bethe ansatz, we determined the eigenvalues of the transfer matrix for small system size by (brute force) numerical diagonalization; the same eigenvalues were obtained by numerically solving the BAE's.

IV. THERMODYNAMICS

We are interested in the behavior of the model as a function of the sublattice densities, that is, the canonical ensemble. In order to set up a transfer matrix, we have passed to the grand canonical ensemble, which is controlled by sublattice weights (or chemical potentials) instead of sublattice densities. In this section it turns out that the transfer matrix leads to a semigrand canonical ensemble. It is controlled partly by densities (essentially the two conserved quantities) and partly by chemical potentials. We describe the Legendre transformation from this ensemble back to the canonical ensemble. We also look into the symmetries between the sublattices and how they appear in the semigrand canonical ensemble.

A. Legendre transformation

In passing to the grand canonical ensemble, each trimer on a sublattice i was given a weight $w_i=\exp(\mu_i)$. Certain combinations of these weights occur in the BAE's (26) and (27) and in the expression (28) of the transfer matrix eigenvalue in terms of the BA roots. It is convenient to assign names to the corresponding combinations of the chemical potentials μ_i,

$$\begin{aligned}
\phi_L &= \tfrac{1}{2}[(3\mu_0-\mu_1-\mu_2+\mu_3+\mu_4-3\mu_5)\\
&\quad +\rho_R(-\mu_0+\mu_1-\mu_2+\mu_3-\mu_4+\mu_5)],\\
\phi_R &= \tfrac{1}{2}[(3\mu_0-3\mu_1+\mu_2+\mu_3-\mu_4-\mu_5)\\
&\quad +\rho_L(-\mu_0+\mu_1-\mu_2+\mu_3-\mu_4+\mu_5)],\\
\mu_L &= \tfrac{1}{4}(-\mu_0-\mu_1-\mu_2+\mu_3+\mu_4+\mu_5),\\
\mu_R &= \tfrac{1}{4}(-\mu_0+\mu_1+\mu_2+\mu_3-\mu_4-\mu_5),
\end{aligned}$$

where $\rho_L=n_L/L$ and $\rho_R=n_R/L$ denote the densities of the particles L and R. With these definitions, the BAE's (26) and (27) can be written

$$(e^{\phi_L}\xi_i)^L = (-)^{n_L+n_R-1}\prod_{j=1}^{n_R}\eta_j^{-1}\frac{\xi_i-\eta_j}{\xi_i+\eta_j^{-1}}, \tag{29}$$

$$(e^{\phi_R}\eta_j)^L = (-)^{L+n_R-1}\prod_{i=1}^{n_L}\xi_i^{-1}\frac{\eta_j-\xi_i}{\eta_j+\xi_i^{-1}}, \tag{30}$$

while the eigenvalue expression (28) becomes

$$\Lambda=\exp(L\mu_0+n_L\mu_L+n_R\mu_R)\left[\prod_{i=1}^{n_L}\xi_i\prod_{j=1}^{n_R}(-\eta_j)\right]^{1/2}. \tag{31}$$

Taking the logarithm, dividing by L, and sending L to infinity gives the free energy per trimer in the thermodynamic limit,

$$\Omega(\rho_L,\rho_R;\mu_0,\mu_1,\ldots,\mu_5) = \Phi(\rho_L,\rho_R;\phi_L,\phi_R)-\rho_L\mu_L-\rho_R\mu_R-\mu_0,$$

where

$$\Phi(\rho_L,\rho_R;\phi_L,\phi_R) = -\lim_{L\to\infty}\frac{1}{L}\ln\left[\prod_{i=1}^{n_L}\xi_i\prod_{j=1}^{n_R}(-\eta_j)\right]^{1/2}. \tag{32}$$

It is the free energy in a semigrand canonical ensemble where the numbers of trimers on the different sublattices may vary but are subject to the constraints imposed by fixing the particle densities [see Eqs. (5) and (6)]. In order to do the Legendre transform to the canonical ensemble, the derivatives of Ω with respect to $\mu_0,\mu_1,\ldots,\mu_5$ have to be taken. This gives the ensemble average densities

$$\rho_0=\left(-\frac{3}{2}+\frac{1}{2}\rho_R\right)\frac{\partial\Phi}{\partial\phi_L}+\left(-\frac{3}{2}+\frac{1}{2}\rho_L\right)\frac{\partial\Phi}{\partial\phi_R}-\frac{1}{4}\rho_L-\frac{1}{4}\rho_R+1, \tag{33}$$

$$\rho_1=\left(+\frac{1}{2}-\frac{1}{2}\rho_R\right)\frac{\partial\Phi}{\partial\phi_L}+\left(+\frac{3}{2}-\frac{1}{2}\rho_L\right)\frac{\partial\Phi}{\partial\phi_R}-\frac{1}{4}\rho_L+\frac{1}{4}\rho_R, \tag{34}$$

$$\rho_2=\left(+\frac{1}{2}+\frac{1}{2}\rho_R\right)\frac{\partial\Phi}{\partial\phi_L}+\left(-\frac{1}{2}+\frac{1}{2}\rho_L\right)\frac{\partial\Phi}{\partial\phi_R}-\frac{1}{4}\rho_L+\frac{1}{4}\rho_R, \tag{35}$$

$$\rho_3=\left(-\frac{1}{2}-\frac{1}{2}\rho_R\right)\frac{\partial\Phi}{\partial\phi_L}+\left(-\frac{1}{2}-\frac{1}{2}\rho_L\right)\frac{\partial\Phi}{\partial\phi_R}+\frac{1}{4}\rho_L+\frac{1}{4}\rho_R, \tag{36}$$

$$\rho_4=\left(-\frac{1}{2}+\frac{1}{2}\rho_R\right)\frac{\partial\Phi}{\partial\phi_L}+\left(+\frac{1}{2}+\frac{1}{2}\rho_L\right)\frac{\partial\Phi}{\partial\phi_R}+\frac{1}{4}\rho_L-\frac{1}{4}\rho_R, \tag{37}$$

$$\rho_5=\left(+\frac{3}{2}-\frac{1}{2}\rho_R\right)\frac{\partial\Phi}{\partial\phi_L}+\left(+\frac{1}{2}-\frac{1}{2}\rho_L\right)\frac{\partial\Phi}{\partial\phi_R}+\frac{1}{4}\rho_L-\frac{1}{4}\rho_R, \tag{38}$$

In Sec. II A it was seen that because the sublattice densities satisfy two constraints, four of them are independent. Equations (33)–(38) express the sublattice densities in terms of only four quantities, namely, ρ_L, ρ_R, $\partial\Phi/\partial\phi_L$, and $\partial\Phi/\partial\phi_R$. Therefore these four quantities must be independent and the sublattice densities given by Eqs. (33)–(38) must satisfy the two constraints (1) and (2). This can also be verified by direct computation. The entropy per trimer is

$$S(\rho_0,\rho_1,\ldots,\rho_5)=-\Omega-\sum_{k=0}^{5}\rho_k\mu_k=-\Phi+\frac{\partial\Phi}{\partial\phi_L}\phi_L+\frac{\partial\Phi}{\partial\phi_R}\phi_R. \tag{39}$$

It is remarkable that the chemical potentials μ_0, μ_L, and μ_R that occur in the expression (31) for the eigenvalue have disappeared in the Legendre transformation. As a consequence, Φ and hence the densities $\rho_0,\rho_1,\ldots,\rho_5$ and the entropy S are now functions of four parameters: the particle densities ρ_L and ρ_R and the potentiallike quantities ϕ_L and ϕ_R. These are just the parameters that govern the BAE's (29) and (30). This agrees with the fact that the canonical ensemble also has four parameters.

B. Symmetries of the parameter space

For the reference state of the BA sublattice 0 was chosen. Since the model is invariant under horizontal translations over a single lattice edge, sublattice 2 (or 4) could have been chosen instead. The original situation can be regained by renumbering the sublattices $i\to i-2$ (mod 6). The sublattice densities ρ_i' in the new numbering are related to the densities ρ_i in the old numbering by

$$\rho_0'=\rho_2,\quad \rho_1'=\rho_3,\quad \text{etc.}$$

and analogously for the chemical potentials μ_i. From this, one computes

$$\rho_L'=2-\rho_R,\quad \rho_R'=1-\rho_R,\quad \phi_L'=-\phi_L+\phi_R,\quad \phi_R'=-\phi_L.$$

Similarly the model is invariant under reflection in a horizontal line. The corresponding sublattice renumbering is $i\to i+3$ (mod 6). This gives

$$\rho_L'=2-\rho_L,\quad \rho_R'=2-\rho_R,\quad \phi_L'=\phi_L,\quad \phi_R'=\phi_R.$$

The model is also invariant under reflection in a vertical line. For the line passing through sublattices 0 and 3, the renumbering is $i\to -i$ (mod 6). Obviously this is nothing but interchanging left and right, so

$$\rho_L'=\rho_R,\quad \rho_R'=\rho_L,\quad \phi_L'=\phi_R,\quad \phi_R'=\phi_L.$$

Together these three transformations generate a group of order 12. In Sec. VI C we shall find four ''families'' of points in the parameter space where the entropy of the model can be computed exactly. These four families are related by symmetries from this group. Finally, the model is invariant under some rotations. As an example, consider the rotation over $2\pi/3$ about an up triangle of the lattice. The odd sublattices are renumbered: $1\to3\to5\to1$ and the even sublattices remain invariant. This does not give a simple transformation of ρ_L, ρ_R, ϕ_L, and ϕ_R because in the definition of these four quantities the direction in which the transfer matrix acts plays a special role. Rotations do not preserve this direction, in contrast to the translation and the two reflections described above. The symmetry group generated by all these operations is of order 36.

V. INTEGRAL EQUATIONS

In Sec. III two sets of BAE's were derived. These equations can be solved numerically for system size L up to a few hundred, say. This can be done essentially in the full parameter space. (The regions where numerical complications arise can be mapped to regions without such difficulties by means of symmetries from Sec. IV B.) We, however, want to get analytic expressions for the physical quantities of the model in thermodynamic limit. In the present section the BAE's in the thermodynamic limit are turned into two integral equations for two complex functions. These functions are multivalued and their monodromy properties are obtained from the integral equations. The functions are then determined from their monodromy and analyticity properties. In the next section these functions will be used to compute physical quantities of the model.

A. Derivation

We shall now in the usual fashion derive integral equations from the BAE's (29) and (30). The logarithmic version of these BAE's is

$$LF_{\mathrm{L}}(\xi_i) \equiv (n_{\mathrm{L}} + n_{\mathrm{R}} - 1)\pi i \pmod{2\pi i}, \tag{40}$$

$$LF_{\mathrm{R}}(\eta_j) \equiv (L + n_{\mathrm{R}} - 1)\pi i \pmod{2\pi i}, \tag{41}$$

where

$$F_{\mathrm{L}}(z) = \ln z - \frac{1}{L}\sum_{j=1}^{n_{\mathrm{R}}} [\ln(z-\eta_j) - \ln(z+\eta_j^{-1})] + \phi_{\mathrm{L}} + \frac{1}{L}\sum_{j=1}^{n_{\mathrm{R}}} \ln \eta_j,$$

$$F_{\mathrm{R}}(z) = \ln z - \frac{1}{L}\sum_{i=1}^{n_{\mathrm{L}}} [\ln(z-\xi_i) - \ln(z+\xi_i^{-1})] + \phi_{\mathrm{R}} + \frac{1}{L}\sum_{i=1}^{n_{\mathrm{L}}} \ln \xi_i. \tag{42}$$

The derivatives of these functions are denoted $f_{\mathrm{L}}(z)$ and $f_{\mathrm{R}}(z)$, respectively.

For the understanding of the structure of the solutions to the BAE's we rely on numerical computations for finite system size. For many values of the parameters ρ_{L}, ρ_{R}, ϕ_{L}, and ϕ_{R} the BA roots for the largest eigenvalue show the following features. The roots ξ_i and η_j lie on smooth curves in the complex plane. When the system size becomes large, these curves tend to well-defined limit shapes. These limit curves will be called Ξ and H. The sets $\{\xi_i\}$ and $\{\eta_j\}$ (and hence also the curves Ξ and H) are invariant under complex conjugation; this implies that

$$f_{\mathrm{L}}(z^*) = f_{\mathrm{L}}(z)^* \quad \text{and} \quad f_{\mathrm{R}}(z^*) = f_{\mathrm{R}}(z)^*. \tag{43}$$

The curve Ξ crosses the positive real axis whereas H crosses the negative real axis. Figure 7 shows the distribution of the roots for the largest eigenvalue in a given sector $n_{\mathrm{L}}, n_{\mathrm{R}}$.

By means of the same arguments as used by Kalugin [16] for the square-triangle tiling, it can be derived that in the thermodynamic limit the derivatives $f_{\mathrm{L}}(z)$ and $f_{\mathrm{R}}(z)$ satisfy the integral equations

$$f_{\mathrm{L}}(z) = \frac{1}{z} + \frac{1}{2\pi i}\int_H \left(\frac{1}{\eta - z} + \frac{1}{\eta^{-1} + z}\right) f_{\mathrm{R}}(\eta)\, d\eta, \tag{44}$$

$$f_{\mathrm{R}}(z) = \frac{1}{z} + \frac{1}{2\pi i}\int_\Xi \left(\frac{1}{\xi - z} + \frac{1}{\xi^{-1} + z}\right) f_{\mathrm{L}}(\xi)\, d\xi. \tag{45}$$

Let b_{L} and b_{R} denote the end points in the upper half plane of Ξ and H, respectively. Then the integration contour Ξ runs from b_{L}^* to b_{L} while H runs from b_{R} to b_{R}^*. From Eqs. (44) and (45), it is seen that $f_{\mathrm{L}}(z)$ has branch cuts H and $-H^{-1}$ and that $f_{\mathrm{R}}(z)$ has branch cuts Ξ and $-\Xi^{-1}$. From the same equations it is easily computed that $z f_{\mathrm{L}}(z)$ and $z f_{\mathrm{R}}(z)$ are invariant under $z \mapsto -z^{-1}$. Therefore we substitute

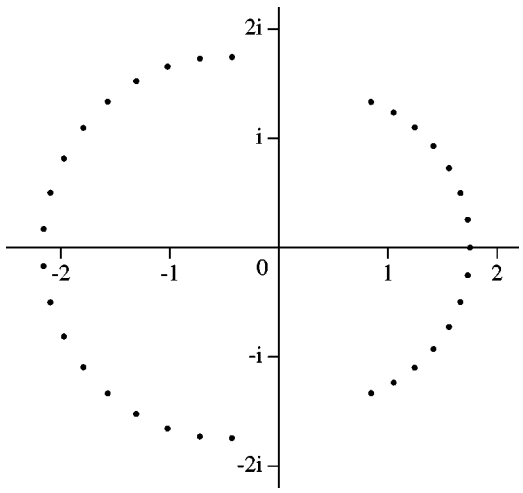

FIG. 7. Distribution of the BAE roots for the largest eigenvalue. The ξ are on the right, the η on the left. (The parameters have the values $\phi_{\mathrm{L}} = -0.46$, $\phi_{\mathrm{R}} = -0.653$, $n_{\mathrm{L}} = 15$, $n_{\mathrm{R}} = 18$, and $L = 30$.)

$$z - z^{-1} = \hat{z} \tag{46}$$

and define

$$g_{\mathrm{L}}(\hat{z}) = z f_{\mathrm{L}}(z) \quad \text{and} \quad g_{\mathrm{R}}(\hat{z}) = z f_{\mathrm{R}}(z). \tag{47}$$

The two branch cuts H and $-H^{-1}$ of $f_{\mathrm{L}}(z)$ then collapse to a single branch cut $\hat{H}$ of $g_{\mathrm{L}}(\hat{z})$ and similarly for $f_{\mathrm{R}}(z)$. Equations (44) and (45) become

$$g_{\mathrm{L}}(\hat{z}) = 1 + \frac{1}{2\pi i}\int_{\hat{H}} \frac{1}{\hat{\eta} - \hat{z}}\, g_{\mathrm{R}}(\hat{\eta})\, d\hat{\eta}, \tag{48}$$

$$g_{\mathrm{R}}(\hat{z}) = 1 + \frac{1}{2\pi i}\int_{\hat{\Xi}} \frac{1}{\hat{\xi} - \hat{z}}\, g_{\mathrm{L}}(\hat{\xi})\, d\hat{\xi}. \tag{49}$$

The functions $f_{\mathrm{L}}(z)$ and $f_{\mathrm{R}}(z)$ and hence also $g_{\mathrm{L}}(\hat{z})$ and $g_{\mathrm{R}}(\hat{z})$ contain all the information about the BA roots ξ_i and η_j that is needed to compute the densities ρ_{L} and ρ_{R}, the phases ϕ_{L} and ϕ_{R}, and the semigrand canonical free energy Φ.

The integral equations (48) and (49) are very similar to the equations obtained by Kalugin [16] for the square-triangle random tiling model. He tackles his equations by exploiting the monodromy properties of the functions. We shall use the same method for our integral equations, closely following Kalugin's argument.

B. Monodromy and analyticity properties

In the remainder of this paper we shall, unless stated otherwise, consider the special case that the end points and $\hat{b}_{\mathrm{L}}$ $\hat{b}_{\mathrm{L}}^*$ of $\hat{\Xi}$ coincide with the end points $\hat{b}_{\mathrm{R}}$ and $\hat{b}_{\mathrm{R}}^*$ of $\hat{H}$, and that the contours do not meet in other points. Following the

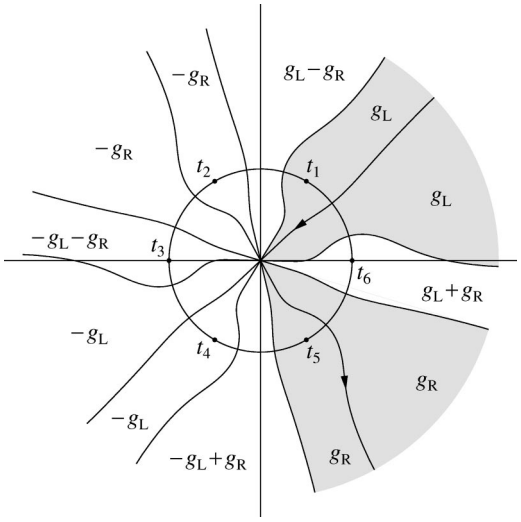

FIG. 8. The complex t plane. The contours corresponding to $\hat{\Xi}$ and $\hat{H}$ divide the plane into sectors that correspond to different branches of the function $g(\hat{z})$. The shaded regions correspond to $g_L(\hat{z})$ and $g_R(\hat{z})$. (The interest of this picture lies in its qualitative features, but it was actually obtained from a numerical solution of the BAE's. The parameters are $\phi_L=-0.46$, $\phi_R=-0.653$, $n_L=152$, $n_R=186$, and $L=200$. These values correspond to $\hat{b}=2ie^{-0.05i}$.)

argument given for the square-triangle tiling by Kalugin [16], one can then show that the functions $g_L(\hat{z})$ and $g_R(\hat{z})$ are different branches of one function $g(\hat{z})$, which is a single-valued function $h(t)$ of the variable

$$t=t(\hat{z})=\left(\frac{\hat{z}-\hat{b}}{\hat{z}-\hat{b}^*}\right)^{1/6}. \tag{50}$$

Kalugin's argument leads to an explicit expression for each of the branches of $g(\hat{z})=h(t)$ in terms of $g_L(\hat{z})$ and $g_R(\hat{z})$. These expressions and the location in the t plane of the branches are shown in Fig. 8. In particular, the branch containing the point $t=e^{-\pi i/3}$ is $g_R(\hat{z})$.

It follows from Eq. (48) that $g_L(\hat{z})$ is analytic everywhere except on the branch cut $\hat{H}$. Similarly, $g_R(\hat{z})$ is analytic everywhere except on $\hat{\Xi}$. In particular, it is analytic on the contour $\hat{H}$, except perhaps at the end points, as these lie also on $\hat{\Xi}$. It then follows from Eq. (48) that $g_L(\hat{z})$ remains finite if $\hat{z}$ approaches a point (not an end point) on its branch cut $\hat{H}$. An analogous statement holds for $g_R(\hat{z})$. To summarize, $g_L(\hat{z})$ and $g_R(\hat{z})$ are finite everywhere except perhaps at $\hat{b}$ and $\hat{b}^*$. Therefore $h(t)$ is analytic everywhere except perhaps at $t=0$ and $t=\infty$. Because $h(t)$ is single valued, it can only have power singularities (with integer exponent). Now

$$\rho_L=\frac{1}{2\pi i}\int_{\Xi} f_L(z)dz$$

$$=\frac{1}{2\pi i}\int_{\hat{\Xi}} g_L(\hat{z})\frac{dz}{d\hat{z}}d\hat{z}=\frac{1}{2\pi i}\int_{\infty}^{0} h(t)\frac{dz}{d\hat{z}}\frac{d\hat{z}}{dt}dt, \tag{51}$$

where the last integral is over some contour running from ∞ to 0, is finite. Since $dz/d\hat{z}$ remains finite and nonzero for t near 0 or ∞, and

$$\frac{d\hat{z}}{dt}=\frac{6(\hat{b}-\hat{b}^*)t^5}{(t^6-1)^2}\sim\begin{cases} t^5, & \text{if } t\to 0 \\ t^{-7}, & \text{if } t\to\infty, \end{cases}$$

it follows that $h(t)$ has, at most, singularities t^{-5} at $t=0$ and t^5 at $t=\infty$. Hence, the 1-form

$$g(\hat{z})d\hat{z}=h(t)\frac{d\hat{z}}{dt}dt \tag{52}$$

is nonsingular at $t=0$ and $t=\infty$.

C. Calculation of $g(\hat{z})$

In the previous subsection it was shown that the 1-form (52) is nonsingular at $t=0$ and $t=\infty$. The only singularities it can have are second-order poles at the zeros $t_1,t_2,\ldots,t_6$ of t^6-1. (These are the points in the t plane corresponding to $\hat{z}=\infty$.) Therefore it can be written as

$$g(\hat{z})d\hat{z}=h(t)\frac{d\hat{z}}{dt}dt=\sum_{k=1}^{6}\left\{\frac{r_k}{t-t_k}+\frac{s_k}{(t-t_k)^2}\right\}dt.$$

The coefficients r_k and s_k are given by

$$r_k=\mathrm{Res}_{t=t_k}h(t)\frac{d\hat{z}}{dt}dt=\mathrm{Res}_{\hat{z}=\infty}g(\hat{z})d\hat{z}$$

and

$$s_k=\mathrm{Res}_{t=t_k}(t-t_k)h(t)\frac{d\hat{z}}{dt}dt$$

$$=[(t-t_k)\hat{z}]_{t=t_k}\mathrm{Res}_{\hat{z}=\infty}\hat{z}^{-1}g(\hat{z})d\hat{z},$$

where the appropriate branch of $g(\hat{z})$ is to be taken.

The residues $\mathrm{Res}_{\hat{z}=\infty}g(\hat{z})d\hat{z}$ and $\mathrm{Res}_{\hat{z}=\infty}\hat{z}^{-1}g(\hat{z})d\hat{z}$ still have to be computed. From Eqs. (48) and (49), one has

$$\mathrm{Res}_{\hat{z}=\infty}g_L(\hat{z})d\hat{z}=-\frac{1}{2\pi i}\int_{\hat{H}}g_R(\hat{\eta})d\hat{\eta}=:R_L,$$

$$\mathrm{Res}_{\hat{z}=\infty}g_R(\hat{z})d\hat{z}=-\frac{1}{2\pi i}\int_{\hat{\Xi}}g_L(\hat{\xi})d\hat{\xi}=:R_R,$$

and

$$\mathrm{Res}_{\hat{z}=\infty}\hat{z}^{-1}g_L(\hat{z})d\hat{z}=-1,$$

$$\mathrm{Res}_{\hat{z}=\infty}\hat{z}^{-1}g_R(\hat{z})d\hat{z}=-1.$$

The residues for the other branches of $g(\hat{z})$ follow directly from the expressions in Fig. 8. They are listed in Table II. It follows from Eq. (43) that the integrals R_L and R_R are real.

Combining these results gives, after some algebra,

TABLE II. The poles and residues of $g(\hat{z})d\hat{z}$.

k	t_k	g	$\mathrm{Res}_{\hat{z}=\infty} g(\hat{z})d\hat{z}$	$\mathrm{Res}_{\hat{z}=\infty}\hat{z}^{-1}g(\hat{z})d\hat{z}$
1	$e^{\pi i/3}$	g_{L}	R_{L}	-1
2	$-e^{-\pi i/3}$	$-g_{\mathrm{R}}$	$-R_{\mathrm{R}}$	1
3	-1	$-g_{\mathrm{L}}-g_{\mathrm{R}}$	$-R_{\mathrm{L}}-R_{\mathrm{R}}$	2
4	$-e^{\pi i/3}$	$-g_{\mathrm{L}}$	$-R_{\mathrm{L}}$	1
5	$e^{-\pi i/3}$	g_{R}	R_{R}	-1
6	1	$g_{\mathrm{L}}+g_{\mathrm{R}}$	$R_{\mathrm{L}}+R_{\mathrm{R}}$	-2

$$g(\hat{z})=\sum_{k=1}^{6}\left\{\frac{r_k}{t-t_k}+\frac{s_k}{(t-t_k)^2}\right\}\left(\frac{d\hat{z}}{dt}\right)^{-1}$$
$$=(1-2C)t+(1-2C^*)t^{-1}+C(t+t^{-5})$$
$$+C^*(t^{-1}+t^5) \tag{53}$$

with

$$C=\frac{1}{6}+\frac{1}{2\sqrt{3}\,\mathrm{Im}\,\hat{b}}[e^{\pi i/3}R_{\mathrm{L}}-e^{-\pi i/3}R_{\mathrm{R}}].$$

We shall now argue in the generic case, $\hat{b}\neq 2i$, that $C=0$. From Eqs. (40) and (41), the curves Ξ and H are described by $\mathrm{Re}[f_{\mathrm{L}}(z)dz]=0$ and $\mathrm{Re}[f_{\mathrm{R}}(z)dz]=0$, respectively, so the corresponding curves in the t plane are both solutions of

$$\mathrm{Re}\left[\frac{g(\hat{z})}{z}\frac{dz}{d\hat{z}}\frac{d\hat{z}}{dt}dt\right]=0. \tag{54}$$

Note that z and $dz/d\hat{z}$ are not single-valued functions of t but the two branches of

$$\frac{1}{z}\frac{dz}{d\hat{z}}=\frac{1}{z+z^{-1}}=\frac{1}{\sqrt{\hat{z}^2+4}}$$

differ only by a sign, which does not influence Eq. (54). The two different solutions of Eq. (54) corresponding to Ξ and H, respectively, meet at $t=0$ (and at $t=\infty$), so at these points the differential equation admits multiple solutions. When $t\to 0$

$$\frac{g(\hat{z})}{z}\frac{dz}{d\hat{z}}\frac{d\hat{z}}{dt}dt=6\frac{\hat{b}-\hat{b}^*}{b+b^{-1}}[C+(1-C^*)t^4+O(t^6)]dt,$$

so this implies that $C=0$.

We shall now argue in the special case $\hat{b}=2i$ that $C=0$. When $t\to 0$

$$f(z)dz=\frac{g(\hat{z})}{z}\frac{dz}{d\hat{z}}\frac{d\hat{z}}{dt}dt=6[Ct^{-3}+(1-C^*)t+O(t^3)]dt$$

(and similarly when $t\to\infty$). The finiteness of the integral (51) (or its analog for ρ_{R}) implies that $C=0$.

Now Eq. (53) becomes

$$g(\hat{z})=t+t^{-1}. \tag{55}$$

The functions $g_{\mathrm{L}}(\hat{z})$ and $g_{\mathrm{R}}(\hat{z})$ are obtained by taking the appropriate branches $t_{\mathrm{L}}(\hat{z})$ and $t_{\mathrm{R}}(\hat{z})$ of $t(\hat{z})$. The branch $t_{\mathrm{L}}(\hat{z})$ is determined by $t_{\mathrm{L}}(\infty)=e^{\pi i/3}$ and the fact that it has $\hat{H}$ as its only branch cut. Similarly, $t_{\mathrm{R}}(\hat{z})$ is determined by $t_{\mathrm{R}}(\infty)=e^{-\pi i/3}$ and the fact that it has $\hat{\Xi}$ as its only branch cut.

VI. CALCULATION OF PHYSICAL QUANTITIES

In Sec. IV the relation was established between the canonical ensemble we are interested in and the semigrand canonical ensemble that arises in the BA from Sec. III. In Sec. V, BA information was encoded in two complex functions satisfying a set of integral equations. These functions were then solved from those equations. In the present section the physical quantities occurring in Sec. IV are extracted from the complex functions determined in Sec. V.

A. Calculation of ρ_{L}, ρ_{R}, ϕ_{L}, ϕ_{R}, and Φ

From Eqs. (47) and (55), $f_{\mathrm{L}}(z)$ and $f_{\mathrm{R}}(z)$ are both given by

$$f(z)=\frac{t+t^{-1}}{z}, \tag{56}$$

with different branches of t. It was claimed in Sec. V A that the BA parameters ρ_{L}, ρ_{R}, ϕ_{L}, and ϕ_{R} and the semigrand canonical-free energy Φ can be computed from the functions $f_{\mathrm{L}}(z)$ and $f_{\mathrm{R}}(z)$. These functions depend on the point $\hat{b}$. The particle density ρ_{L} was already computed in Eq. (51),

$$\rho_{\mathrm{L}}=\frac{1}{2\pi i}\int_{\Xi}f_{\mathrm{L}}(z)dz. \tag{57}$$

Because $f_{\mathrm{L}}(z)$ is analytic, this integral does not depend on the precise shape of Ξ but on its homology only.

Next ϕ_{L} is calculated. Since $f_{\mathrm{L}}(z)$ is known, the function $F_{\mathrm{L}}(z)$ is determined up to an integration constant. The real part of this integration constant is fixed by $\mathrm{Re}\,F_{\mathrm{L}}(b_{\mathrm{L}})=0$, Eq. (40). From Eq. (42), one has

$$\mathrm{Re}[F_{\mathrm{L}}(z)+F_{\mathrm{L}}(-z^{-1})]=2\phi_{\mathrm{L}}.$$

It is now easy to compute that

$$\phi_{\mathrm{L}}=\frac{1}{2}\mathrm{Re}\int_{b_{\mathrm{L}}}^{-b_{\mathrm{L}}^{-1}}f_{\mathrm{L}}(z)dz. \tag{58}$$

From Eq. (32) the free energy Φ equals $-(\Sigma_{\mathrm{L}}+\Sigma_{\mathrm{R}})$ with

$$\Sigma_{\mathrm{L}}=\lim_{L\to\infty}\frac{1}{2}\frac{1}{L}\sum_{j=1}^{n_{\mathrm{R}}}\ln|\eta_j|$$

and analogously for Σ_{R}. Using Eq. (42), one calculates

$$\Sigma_{\mathrm{L}} = \mathrm{Re}[F_{\mathrm{L}}(z) - \ln z]\big|_0^\infty = \frac{1}{4}\,\mathrm{Re}\int_0^\infty \left(f_{\mathrm{L}}(z) - \frac{1}{z} \right) dz. \tag{59}$$

In Eqs. (58) and (59), the integral again only depends on the homology of the integration path, not on its precise shape. The real part of the integral even does not depend at all on the path chosen between the integration end points, but the imaginary part does. This is because the indefinite integral (42) is a sum of logarithms with real prefactors, and distinct branches of a logarithm differ by a multiple of $2\pi i$, which is purely imaginary.

Replacing in Eqs. (57), (58), and (59) all subscripts L with R and in Eq. (57), the integration contour Ξ with H yields expressions of ρ_{R}, ϕ_{R}, and Σ_{R} as integrals of functions involving $f_{\mathrm{R}}(z)$. These integrals for ρ_{L}, ρ_{R}, ϕ_{L}, ϕ_{R}, Σ_{L}, and Σ_{R} are of the form $\int y\,dz$, where the points (y, z) lie on an algebraic curve of genus 5. Therefore the indefinite integrals cannot be expressed in terms of ''standard'' functions. This does not prove that the definite integrals we need cannot be expressed in terms of standard functions, but it seems unlikely. Of course they can be evaluated numerically.

B. Calculation of $\partial\Phi/\partial\phi_{\mathrm{L}}$ and $\partial\Phi/\partial\phi_{\mathrm{R}}$

The Legendre transformation in Sec. IV A involves the derivatives $\partial\Phi/\partial\phi_{\mathrm{L}}$ and $\partial\Phi/\partial\phi_{\mathrm{R}}$. Unfortunately, we have not been able to compute Φ as a function of ρ_{L}, ρ_{R}, ϕ_{L}, and ϕ_{R} for all values of these arguments. Instead, we have in Sec. VI A computed these parameters and the free energy in the case that the curves $\hat{\Xi}$ and $\hat{H}$ close, as a function of their common end point $\hat{b} = \hat{b}_{\mathrm{L}} = \hat{b}_{\mathrm{R}}$. In order to still obtain the derivatives $\partial\Phi/\partial\phi_{\mathrm{L}}$ and $\partial\Phi/\partial\phi_{\mathrm{R}}$, we resort to a perturbation analysis. The details can be found in the Appendix; here we only give some results. An infinitesimally small complex parameter C describes how far the curves open up. The thermodynamic parameters $\rho_{\mathrm{L}}, \rho_{\mathrm{R}}, \phi_{\mathrm{L}}, \phi_{\mathrm{R}}$ and the free energy Φ then are functions of $\hat{b}$ and C. If all their first-order partial derivatives are known, $\partial\Phi/\partial\phi_{\mathrm{L}}$ and $\partial\Phi/\partial\phi_{\mathrm{R}}$ can be found by applying the standard coordinate-transformation formula to the transformation between coordinates $\mathrm{Re}\,\hat{b}$, $\mathrm{Im}\,\hat{b}$, $\mathrm{Re}\,C$, and $\mathrm{Im}\,C$ on one hand and ρ_{L}, ρ_{R}, ϕ_{L}, and ϕ_{R} on the other. The derivatives with respect to $\mathrm{Re}\,\hat{b}$ and $\mathrm{Im}\,\hat{b}$ can be obtained immediately from the integral expressions in Sec. VI A. For the derivatives with respect to $\mathrm{Re}\,C$ and $\mathrm{Im}\,C$, the perturbation analysis is needed. It tells that to leading order in C the parameters $\rho_{\mathrm{L}}, \rho_{\mathrm{R}}, \phi_{\mathrm{L}}, \phi_{\mathrm{R}}$ and the free energy $\Phi = -(\Sigma_{\mathrm{L}} + \Sigma_{\mathrm{R}})$ are again given by the integrals (57), (58), and (59), and their analogs involving $f_{\mathrm{R}}(z)$, where $f(z)$ is now given by

$$f(z) = \frac{t + t^{-1} + C(t^{-5} - t) + C^*(t^5 - t^{-1})}{z}. \tag{60}$$

This yields integral expressions for their derivatives with respect to $\mathrm{Re}\,C$ and $\mathrm{Im}\,C$.

The expressions thus obtained for the partial derivatives of ρ_{L}, ρ_{R}, ϕ_{L}, ϕ_{R}, and Φ with respect to $\mathrm{Re}\,\hat{b}$, $\mathrm{Im}\,\hat{b}$, $\mathrm{Re}\,C$, and $\mathrm{Im}\,C$ were evaluated numerically for some chosen value of $\hat{b}$, and from this $\partial\Phi/\partial\phi_{\mathrm{L}}$ and $\partial\Phi/\partial\phi_{\mathrm{R}}$ were calculated. These derivatives were also computed from numerical solutions of the BAE's for large system size L by numerical differentiation. The results from the two methods agree, which support the perturbation analysis of the Appendix.

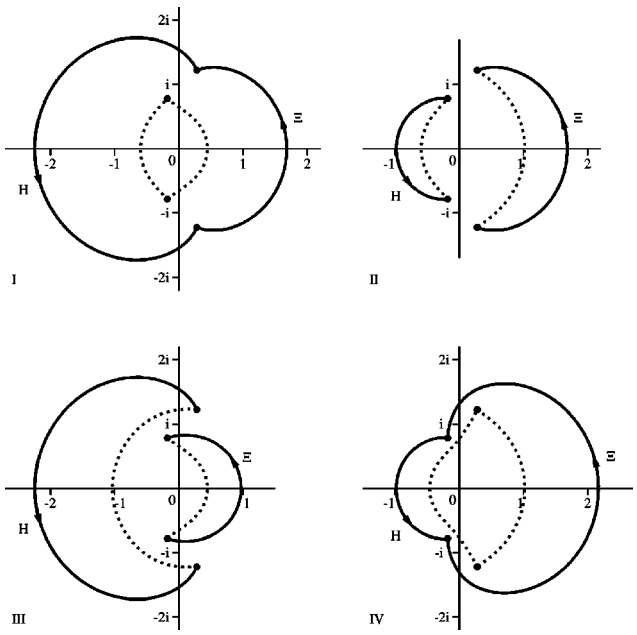

FIG. 9. Four possible configurations of the curves Ξ and H. The dashed curved are $-\Xi^{-1}$ and $-H^{-1}$. In cases I and IV, Ξ and H have the same end points. In cases II and III, Ξ and $-H^{-1}$ share end points, as do H and $-\Xi^{-1}$.

C. Configuration of Ξ and H

In the previous two sections several physical quantities have been expressed as integrals of functions involving $f_{\mathrm{L}}(z)$ and $f_{\mathrm{R}}(z)$. These integrals depend on the parameter $\hat{b}$ and on the topology of the curves Ξ and H, but not on their precise shape. If $\hat{b} \neq 2i$ there are two distinct points in the z plane corresponding to $\hat{b}$, say b_1 and b_2. The end points of Ξ could be b_1 and b_1^* or b_2 and b_2^*, and the same holds for H. Therefore one can expect at least four different configurations for one and the same value of $\hat{b}$. In order to determine what these four configurations actually are, we first guessed what they might look like. Then we chose some particular value of $\hat{b}$ (close to $2i$) and for each of the four expected cases computed the value of the particle densities ρ_{L} and ρ_{R} and the phases ϕ_{L} and ϕ_{R}. The BAE's were solved numerically for these parameter values, for large system size L. The resulting curves followed by ξ and η display indeed the presupposed configurations. These curves are shown in Fig. 9. Note that without first guessing the configurations we would have had no way to find the values of the parameters ρ_{L}, ρ_{R}, ϕ_{L}, and ϕ_{R}, so there would have been no BAE's to solve numerically.

The numerical results show that these four cases are related by the symmetries of the parameter space discussed in

TABLE III. The regions in parameter space of the sublattice densities for cases I–IV and I′–IV′.

$\lvert b_L\rvert$	$\lvert b_R\rvert$			$\mathrm{Re}\,\hat{b}>0$		$\mathrm{Re}\,\hat{b}<0$
>1	>1	$\rho_0=\rho_2=\rho_4$	I	$\rho_1>\rho_5>\rho_3$	I′	$\rho_5>\rho_1>\rho_3$
>1	<1	$\rho_1=\rho_3=\rho_5$	II	$\rho_0>\rho_2>\rho_4$	III′	$\rho_4>\rho_0>\rho_2$
<1	>1	$\rho_1=\rho_3=\rho_5$	III	$\rho_2>\rho_0>\rho_4$	II′	$\rho_0>\rho_4>\rho_2$
<1	<1	$\rho_0=\rho_2=\rho_4$	IV	$\rho_5>\rho_3>\rho_1$	IV′	$\rho_1>\rho_3>\rho_5$

Sec. IV B. They are in a single orbit of the subgroup of order six generated by the horizontal translation (which is of order three) and the product of the reflection in a horizontal line and the reflection in a vertical line (which is of order two). For the remaining two members of this orbit we have not been able to numerically solve the BAE's. In these cases the particle densities are fairly high; we suppose that the curves Ξ and H would cross or otherwise violate the condition that $\hat{\Xi}$ and $\hat{H}$ only share their end points.

Once this symmetry is known, a (numerical) calculation of the physical quantities needs to be carried out only for one of the four cases I–IV. The values for the other three cases are then obtained at once by application of the symmetry transformations.

D. Calculation of the sublattice densities and the entropy

In Sec. VI A the physical quantities ρ_L, ρ_R, ϕ_L, ϕ_R, and Φ pertaining to the semigrand canonical ensemble were calculated from the functions $f_L(z)$ and $f_R(z)$. In Sec. V B the derivatives $\partial\Phi/\partial\phi_L$ and $\partial\Phi/\partial\phi_R$ were computed. Substitution of these results into formulas (33)–(38) and Eq. (39) from Sec. IV A gives the sublattice densities and the entropy, physical quantities for the canonical ensemble. This was performed numerically for a particular value of $\hat{b}$. The results reveal that $\rho_0=\rho_2=\rho_4$ in cases I and IV and $\rho_1=\rho_3=\rho_5$ in cases II and III. From the expressions (33)–(38) for the sublattice densities, this is equivalent to

$$\frac{\partial\Phi}{\partial\phi_L}=\tfrac{1}{6}(2+\rho_L-2\rho_R) \quad \text{and} \quad \frac{\partial\Phi}{\partial\phi_R}=\tfrac{1}{6}(2-2\rho_L+\rho_R) \tag{61}$$

in cases I and IV and

$$\frac{\partial\Phi}{\partial\phi_L}=\tfrac{1}{6}(-\rho_L+2\rho_R) \quad \text{and} \quad \frac{\partial\Phi}{\partial\phi_R}=\tfrac{1}{6}(2\rho_L-\rho_R) \tag{62}$$

in cases II and III. One might hope to derive these expressions analytically from the results of Subsection VI A and VI B. We have not tried this because it would involve rather cumbersome relations among integrals (57), (58), and (59). Once the expressions (61) and (62) have been accepted, the perturbation analysis approach from Sec. VI B becomes superfluous. Substituting them into Eqs. (33)–(38) and Eq. (39) yields new expressions for the sublattice densities and the entropy. The expressions for the sublattice densities are polynomials in the particle densities ρ_L and ρ_R, the expression for the entropy also contains the phases ϕ_L and ϕ_R and of course the free energy Φ.

Cases I–IV correspond to different regions in the parameter space of sublattice densities, as given in Table III. These four cases are defined for $\mathrm{Re}\,\hat{b}>0$ by Fig. 9. The mirror images (with respect to the imaginary axis) of the configurations in Fig. 9 define cases I′–IV′ for $\mathrm{Re}\,\hat{b}<0$. For example, the locus of Ξ (H) for case I′ is the mirror image of the locus of H (Ξ) for case I. Table III also lists the regions in the parameter space of sublattice densities corresponding to the cases I′–IV′.

E. Summary

In the foregoing section an exact solution of the trimer model was derived. Because the results are obtained in the course of a long derivation, we here provide a guide through them. The final result is the entropy as a function of six sublattice densities ρ_i defined in Sec. II A. Complete coverage of the lattice (1) and a further geometric constraint (2) (derived in Sec. II E) leave four independent parameters. A full analytic solution in the thermodynamic limit is obtained in a two-parameter subspace.

The four-dimensional parameter space is described by new variables ρ_L, ρ_R, ϕ_L, and ϕ_R. The free-energy function of the ensemble with these parameters is denoted by Φ. The sublattice densities are expressed in ρ_L, ρ_R, $\partial\Phi/\partial\phi_L$, and $\partial\Phi/\partial\phi_R$ in Eqs. (33)–(38); the entropy is given in terms of Φ, ϕ_L, ϕ_R, $\partial\Phi/\partial\phi_L$, and $\partial\Phi/\partial\phi_R$ in Eq. (39).

The free energy is written as a sum, $\Phi=-(\Sigma_L+\Sigma_R)$. In the solvable subspace the quantities ρ_L, ϕ_L, and Σ_L are expressed as contour integrals of a function $f_L(z)$ in Eqs. (57)–(59). Analogously, the quantities ρ_R, ϕ_R, and Σ_R are integrals of a function $f_R(z)$. The integration paths in the integral (57) for ρ_L and its analog for ρ_R are contours Ξ and H, respectively. These contours are symmetric under complex conjugation. Their end points in the upper half plane are denoted b_L and b_R, respectively. These satisfy the equality $b_L-b_L^{-1}=b_R-b_R^{-1}=\hat{b}$. For each value of $\hat{b}$ (except $\hat{b}=2i$) this equation has two distinct solutions for b_L and for b_R resulting in four configurations I–IV of Ξ and H shown in Fig. 9. The derivatives $\partial\Phi/\partial\phi_L$ and $\partial\Phi/\partial\phi_R$ are given by Eq. (61) in the cases I and IV and by Eq. (62) in the cases II and III.

The functions $f_L(z)$ and $f_R(z)$ are different branches of a function $f(z)$. The branch cuts of $f_L(z)$ are H and $-H^{-1}$ and $f_R(z)$ has branch cuts Ξ and $-\Xi^{-1}$. In terms of a new variable t, defined by Eqs. (46) and (50), the function $f(z)$ is single valued. It is given by Eq. (56), while the functions $f_L(z)$ and $f_R(z)$ are recovered by selecting the appropriate branch $t_L(z)$ and $t_R(z)$ of t, specified at the end of Sec. V C.

VII. PHASE DIAGRAM

In Secs. II A and II E, a linear and a quadratic constraint on the six sublattice densities were derived. In this section we first show that these constraints imply a breaking of the symmetry between certain sublattices. This symmetry breaking suggests that a phase transition takes place when the total density $\rho_\nabla=\rho_1+\rho_3+\rho_5$ of down trimers is increased from 0 to 1. Next we compute the entropy as a function of ρ_∇ from the exact solution of this model. From this entropy the phase diagram of the model in the parameter ρ_∇ is obtained. It is also formulated in terms of the chemical potential of the down trimers instead of their density.

A. Symmetry breaking

The linear constraint (1) on the sublattice densities can be rewritten as

$$\rho_0+\rho_2+\rho_4=1-\rho_\nabla, \tag{63}$$

and from the quadratic constraint (2) one has

$$\rho_0\rho_2+\rho_2\rho_4+\rho_4\rho_0\leqslant\tfrac{1}{3}\rho_\nabla^2 \tag{64}$$

with equality if and only if $\rho_1=\rho_3=\rho_5=\frac{1}{3}\rho_\nabla$. If ρ_∇ is small (to be precise, smaller than $2\sqrt{3}-3$), it follows from Eqs. (63) and (64) that one of ρ_0, ρ_2, and ρ_4 is larger than the other two, say, $\rho_0>\rho_2,\rho_4$. Thus the symmetry between the sublattice 0, 2, and 4 is broken. If there is no further symmetry breaking then $\rho_2=\rho_4$ and $\rho_1=\rho_3=\rho_5$, so

$$\rho_0>\rho_1=\rho_3=\rho_5>\rho_2=\rho_4. \tag{65}$$

By the same token the symmetry between the sublattices 1, 3, and 5 is broken when ρ_∇ is close to 1. When ρ_∇ is increased from 0 to 1 the following seems to be the simplest possible scenario. At $\rho_\nabla=0$, sublattice 0 is fully occupied and the other sublattices are empty. The six sublattice densities change continuously with ρ_∇, and Eq. (65) holds up to $\rho_\nabla=\frac{1}{2}$. There the six sublattice densities are all equal to $\frac{1}{6}$. Then one of the odd sublattices, say 3, takes over and

$$\rho_3>\rho_0=\rho_2=\rho_4>\rho_1=\rho_5$$

all the way to $\rho_\nabla=1$ where all trimers sit on sublattice 3.

B. Entropy for ρ_∇

In the previous subsection the occurrence was suggested of a phase transition when ρ_∇ is increased from 0 to 1. For the study of such a phase transition it would be helpful to know the entropy of the model as a function of $\rho_\nabla=\rho_1+\rho_3+\rho_5$. However, what we have computed thus far is the entropy as a function of all sublattice densities, but only for a two-dimensional subspace. Therefore, for a given ρ_∇ the sublattice densities have to be determined for which the entropy is maximal. If we are fortunate these sublattice densities happen to lie in the two-dimensional solved subspace.

For a given $\rho_\nabla<\frac{1}{2}$, the most symmetric possibility for the six sublattice densities is described by Eq. (65). Another possibility,

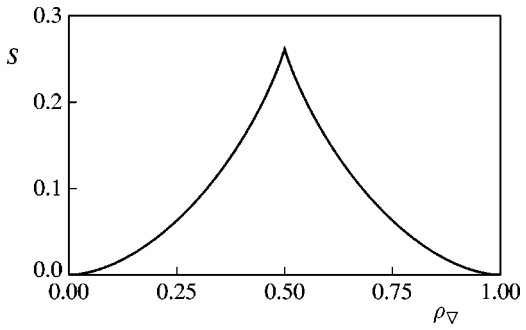

FIG. 10. The entropy per trimer S as a function of the total density of down trimers $\rho_\nabla=\rho_1+\rho_3+\rho_5$. It is obtained from the exact solution in the special case (65) for $\rho_\nabla\leqslant\frac{1}{2}$ and similarly for $\rho_\nabla\geqslant\frac{1}{2}$.

$$\rho_2=\rho_4>\rho_1=\rho_3=\rho_5>\rho_0, \tag{66}$$

exists when $2\sqrt{3}-3\leqslant\rho_\nabla<\frac{1}{2}$. Because of symmetry, Eqs. (65) and (66) are stationary points of the entropy. It is tempting to believe that Eq. (65), being the more general of the two most symmetric cases, corresponds to the maximum of the entropy. By numerically solving the BAE's, the entropy of the model can be computed to high precision. Such calculations confirm that for $\rho_\nabla<\frac{1}{2}$, the entropy takes its maximum at the symmetric case (65) of the sublattice densities, hence within the solvable subspace.

As seen in Sec. VI D for the solvable subspace one has $\rho_0=\rho_2=\rho_4$ in cases I and IV and $\rho_1=\rho_3=\rho_5$ in cases II and III. Consider case II and take $\hat{b}$ on the imaginary axis between 0 and $2i$. The contours $\hat{\Xi}$ and $\hat{H}$ then lie symmetric with respect to the imaginary axis, so $\rho_L=\rho_R$ and hence $\rho_2=\rho_4$. Thus this is precisely the symmetric case (65). Therefore we have obtained the entropy as a function of ρ_∇ for $\rho_\nabla<\frac{1}{2}$. The entropy for $\rho_\nabla>\frac{1}{2}$ follows immediately by the symmetry between up and down trimers. This entropy can also be obtained by considering case I and taking $\hat{b}$ above $2i$ on the imaginary axis. The resulting entropy is shown in Fig. 10. When in case II, $\hat{b}$ is not taken on the imaginary axis between 0 and $2i$, $\rho_2\neq\rho_4$. Figure 11 shows the entropy as a

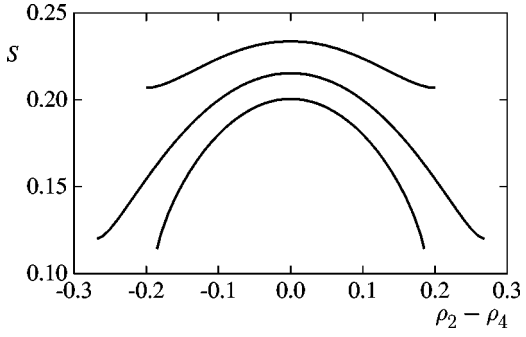

FIG. 11. The entropy per trimer S as a function of $\rho_2-\rho_4$ at fixed $\rho_1=\rho_3=\rho_5$. The end points of the lower curve ($\rho_\nabla=0.45$) are determined by $\rho_2=0$ and by $\rho_4=0$. The upper curve ($\rho_\nabla=0.48$) terminates when $\rho_4=\rho_0$ and when $\rho_2=\rho_0$. At the left end point of the middle curve ($\rho_\nabla=2\sqrt{3}-3\approx0.4641$) $\rho_2=0$ and $\rho_4=\rho_0$, at the right end point $\rho_4=0$ and $\rho_2=\rho_0$.

function of the asymmetry $\rho_2-\rho_4$ at fixed $\rho_1=\rho_3=\rho_5$ along the line determined by the constraints (1) and (2).

For $\hat{b}=2i$, all four cases I, II, III, and IV coincide. The integrals in Sec. VI A then simplify. The sublattice densities are all equal to $\frac{1}{6}$ and the entropy per trimer is $S_{\rm sym}=\ln\frac{4}{3}\sqrt{3}$.

C. Phase transition

Consider a system with ρ_∇ between 0 and $\frac{1}{2}$. The energy is a convex function of ρ_∇, so the system is thermodynamically unstable. It would separate into a frozen phase with $\rho_\nabla=0$ and the symmetric phase with $\rho_\nabla=\frac{1}{2}$. However an interface between these two phases is not possible in the model. Similarly, a system with ρ_∇ between $\frac{1}{2}$ and 1 would demix into phases with $\rho_\nabla=\frac{1}{2}$ and $\rho_\nabla=1$ if coexistence between these phases were possible.

Now give a chemical potential μ_∇ to the down trimers instead of imposing their density ρ_∇. The free energy

$$F=-\mu_\nabla\rho_\nabla-S(\rho_\nabla)$$

takes its global minimum at

$$\rho_\nabla=\begin{cases}0 & \text{for } \mu_\nabla\leqslant-2S_{\rm sym}\\ \frac{1}{2} & \text{for } -2S_{\rm sym}\leqslant\mu_\nabla\leqslant2S_{\rm sym}.\\ 1 & \text{for } 2S_{\rm sym}\leqslant\mu_\nabla\end{cases}$$

Therefore the model is in a frozen phase for $\mu_\nabla<-2S_{\rm sym}$ and for $\mu_\nabla>2S_{\rm sym}$ and in the symmetric phase for $-2S_{\rm sym}<\mu_\nabla<2S_{\rm sym}$. At $\mu_\nabla=-2S_{\rm sym}$, and at $\mu_\nabla=2S_{\rm sym}$ there is coexistence between a frozen and a symmetric phase.

VIII. CONCLUSION

We have introduced a different simple lattice model. It is a fluid of particles each occupying three sites of the triangular lattice. We distinguish six sublattices of adsorption sites for the trimers. Full occupancy and a resulting geometric constraint leave of the six sublattice densities four independent parameters.

In the full four-dimensional parameter space the model is solvable by the Bethe ansatz. In the thermodynamic limit the Bethe ansatz equations can be reduced to two integral equations. In a two-dimensional subspace of the sublattice densities, these integral equations can be solved by means of monodromy and analyticity properties of the functions involved. Within this subspace the entropy and the sublattice densities are given as integral expressions.

The solution is very similar to that of the square-triangle random tiling model [15,16]. In both these cases the solution is closely connected to the hexagonal domain-wall structure of the model. Another solvable model with such a domain-wall structure is the three-coloring model on the honeycomb lattice [20]. In a configuration of this model the edges of the honeycomb lattice are coloured with three colors in such a way that the three edges meeting in each vertex have different colors. Alternatively this model can be formulated as the zero-temperature antiferromagnetic three-state Potts model on the *Kagomé* lattice [21,22]. We shall now briefly discuss the relation between these three models.

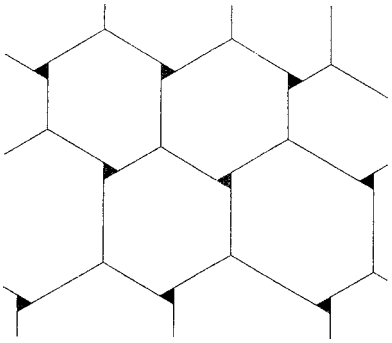

FIG. 12. Schematic representation of the domain-wall structure of the trimer model. The Y joints of the domain walls come in two types. These are mirror images, featuring either a ◀ or a ▶. In contrast, there is only one type of inverted Y joints.

The domain-wall structure of the trimer model is depicted schematically in Fig. 12. It contains two types of Y joints but only one type of inverted Y joints. In the square-triangle tiling, there is only one type of Y joints and one type of inverted Y joints. In the honeycomb lattice three-coloring model, on the other hand, both the Y joints and the inverted Y joints come in two types. Hence these three models appear to be different.

The $A_2^{(1)}$ model is a vertex model on the square lattice derived from an affine Lie algebra [23,24]. It satisfies the Yang-Baxter equation [25,26], so it can be solved by algebraic Bethe ansatz [27]. At a special value of the spectral parameter it is the three-coloring model on the honeycomb lattice [28]. For a suitable choice of the remaining parameters, one of the two types of Y joints and inverted Y joints in the domain-wall network is excluded. In this limit the model is just the square-triangle tiling. This mapping ''explains'' the solvability of the square-triangle tiling in terms of that of the $A_2^{(1)}$ model [29].

In a similar fashion the square-triangle tiling can also be obtained from the trimer model. When the trimers on sublattice 4 (or 2) are excluded, one (or the other) type of Y joint no longer occurs in the domain-wall network. Again the square-triangle tiling results. The Bethe ansatz for the trimer model remains valid in this special case. However, the substitutions (25) no longer makes sense when $w_4=0$ (or $w_2=0$), so the same is true of the analysis in the subsequent sections.

Therefore the three models are connected in sense that both the trimer model and the $A_2^{(1)}$ model contain the square-triangle random tiling as a singular limit. It would be interesting to know if the trimer model, like the square-triangle tiling, is a special case of some model satisfying the Yang-Baxter equation.

ACKNOWLEDGMENTS

We are grateful to Jan de Gier for many useful discussions as well as for putting at our disposal his computer program for numerical Bethe ansatz calculations. We thank

Dave Rusin for enlightening us on the question whether the integrals from Sec. VI A can be expressed in closed form. This work is part of the research program of the ''Stichting voor Fundamenteel Onderzoek der Materie (FOM),'' which is financially supported by the ''Nederlandse Organisatie voor Wetenschappelijk Onderzoek (NWO).''

APPENDIX: PERTURBATION ANALYSIS

In Sec. VI A, the quantities ρ_L, ρ_R, ϕ_L, ϕ_R, and $\Phi=-(\Sigma_L+\Sigma_R)$ were obtained as functions of $\hat{b}=\hat{b}_L=\hat{b}_R$. For the computation of the sublattice densities and the entropy, the derivatives

$$\left(\frac{\partial\Phi}{\partial\phi_L}\right)_{\rho_L\rho_R\phi_R} \quad \text{and} \quad \left(\frac{\partial\Phi}{\partial\phi_R}\right)_{\rho_L\rho_R\phi_L}$$

are also needed as functions of $\hat{b}$. These cannot be calculated by differentiation of the Φ already obtained, because variation of ϕ_L (ϕ_R) at constant ρ_L, ρ_R and ϕ_R (ϕ_L) breaks the condition $\hat{b}_L=\hat{b}_R$. Therefore in this appendix we infinitesimally relax that condition and compute ρ_L, ρ_R, ϕ_L, ϕ_R, and $\Phi=-(\Sigma_L+\Sigma_R)$ to leading order in the infinitesimal relaxation parameter.

When the curves $\hat{\Xi}$ and $\hat{H}$ do not close, $g_L(\hat{z})$ and $g_R(\hat{z})$ are no longer single-valued functions of the variable t. Kalugin [16] has provided a perturbation analysis for the analogous situation in the square-triangle random tiling model. It leans heavily on the understanding of the structure of the Riemann surface of the functions. Our approach does not require such knowledge and is more systematic.

Although $g_L(\hat{z})$ and $g_R(\hat{z})$ are no longer single-valued functions of the variable t, one can still perform the variable transformation (50). The end points $\hat{b}_L$ and $\hat{b}_L^*$ of $\hat{\Xi}$ ($\hat{b}_R$ and $\hat{b}_R^*$ of $\hat{H}$) then correspond to points d_L and d_L^{*-1} (d_R and d_R^{*-1}) in the t plane. The point $\hat{b}$ in Eq. (50) can be chosen such that $|d_L|=|d_R|$; we write

$$d_L=\beta_L\delta \quad \text{and} \quad d_R=\beta_R\delta,$$

with δ real and positive and $|\beta_L|=|\beta_R|=1$. The curves corresponding to $\hat{\Xi}$ and $\hat{H}$ divide the annulus $\delta<|t|<\delta^{-1}$ into sectors, much as in Fig. 8. We get a single-valued function $h(t)=g(\hat{z})$ in this annulus instead of in the whole t plane. Since it is analytic in the annulus it can be expanded as a Laurent series in t,

$$g(\hat{z})=h(t)=\sum_{p=-\infty}^{\infty}A_p t^p. \tag{A1}$$

Figure 8 shows that $h(t)+h(-t)=0$ and that $h(t)+h(te^{2\pi i/3})+h(te^{-2\pi i/3})=0$, so that $A_p=0$ unless $p\equiv\pm1 \pmod 6$. From Eq. (43) one has

$$h(t^{*-1})=g(\hat{z}^*)=g(\hat{z})^*=h(t)^*,$$

so the coefficients A_p satisfy

$$A_{-p}=A_p^*. \tag{A2}$$

We want to view the function $g(\hat{z})$ given by Eq. (A1) as a perturbation around the function $g(\hat{z})$ given by Eq. (55), where δ is the small parameter. In our notation we have suppressed the dependence of the coefficients A_p on δ, β_L, and β_R.

The function $g(\hat{z})$ satisfies the integral equation (48). We investigate how each of the terms t^p from the Laurent series (A1) of $g(\hat{z})$ behaves in this equation. In order to compute the integral we change from $\hat{\eta}$ to $\tau=t(\hat{\eta})$ defined by Eq. (50) as integration variable. The resulting integrand is a rational function in τ, which we decompose into partial fractions. Integration yields polynomial as well as logarithmic terms; some care is required in choosing the branch of the logarithms. Finally we expand in powers of δ, obtaining

$$\begin{aligned}\frac{1}{2\pi i}\int_{\hat{H}}\frac{1}{\hat{\eta}-\hat{z}}\,\tau^p d\hat{\eta} &= t^p - t_1^p + \frac{6}{2\pi i}\left\{\sum_{q=-\infty}^{-1}\frac{\beta_R^{p-6q}}{p-6q}(t^{6q}-1)\,\delta^{p-6q}\right.\\ &\left.+\sum_{q=1}^{\infty}\frac{\beta_R^{p-6q}}{p-6q}(t^{6q}-1)\,\delta^{6q-p}\right\}\end{aligned} \tag{A3}$$

for each term t^p in the Laurent series (A1). Here t in the RHS corresponding to $\hat{z}$ in the LHS is in the sector containing t_1, that is, the sector where $g(\hat{z})$ equals $g_L(\hat{z})$. Comparison with the integral equation (48) shows the following. The term t^p in the RHS of Eq. (A3) exactly matches the term $g_L(\hat{z})$ in the LHS of Eq. (48). The inhomogeneous term $-t_1^p$ in the RHS of Eq. (A3) corresponds to the inhomogeneous term 1 in the integral equation. The other terms in the RHS of Eq. (A3) are ''unwanted''; the powers of t they involve are multiples of 6. Because the Laurent series (A1) satisfies the integral equation (48), the inhomogeneous terms $-t_1^p$ from Eq. (A3) counterbalance the inhomogeneous term 1 of the integral equation,

$$\sum_{p=-\infty}^{\infty}t_1^p A_p=1, \tag{A4}$$

[which means that $g_L(\infty)=1$], and the unwanted terms cancel,

$$\sum_{p=-\infty}^{\infty}\frac{\beta_R^p}{p-6q}\,\delta^p A_p=0, \quad \text{for all } q<0, \tag{A5}$$

$$\sum_{p=-\infty}^{\infty}\frac{\beta_R^p}{p-6q}\,\delta^{-p} A_p=0, \quad \text{for all } q>0. \tag{A6}$$

[Due to Eq. (A2), the equations for q and $-q$ are equivalent.] The function $g(\hat{z})$ also satisfies the integral equation (49); this leads to another similar set of conditions on the coefficients A_p.

The form of Eqs. (A5) and (A6) and their analog from (49) suggests that for β_L and β_R fixed, the coefficients A_p should be power series in δ,

$$A_p = A_p^{(0)} + A_p^{(1)}\delta + A_p^{(2)}\delta^2 + \cdots . \tag{A7}$$

We would like to determine the coefficients $A_p^{(h)}$.

When t approaches the boundary of the annulus, $|t| \to \delta$ or $|t| \to \delta^{-1}$, the unperturbed function $g(\hat{z})$ given by Eq. (55) becomes of the order δ. It seems reasonable to assume that the terms $A_p t^p$ of the perturbed function $g(\hat{z})$ do not grow faster than this, so the coefficients $A_p^{(h)}$ with $h < |p| - 1$ must be zero.

Consider Eq. (A4) and its analog from (49). Substitution of the power series (A7) yields, after rearrangement of the terms,

$$\sum_{h=0}^{\infty} \delta^h \left(\sum_{p=-(h+1)}^{h+1} t_k^p A_p^{(h)} \right) = 1 \quad \text{for} \quad k = 1,5. \tag{A8}$$

The δ^0 part gives

$$t_k A_1^{(0)} + t_k^{-1} A_{-1}^{(0)} = 1, \quad \text{for} \quad k = 1,5.$$

The unique solution of these equations reproduces the unperturbed function $g(\hat{z})$ given by Eq. (55). For $1 \leqslant h \leqslant 3$ the δ^h part of Eq. (A8) gives

$$t_k A_1^{(h)} + t_k^{-1} A_{-1}^{(h)} = 0, \quad \text{for} \quad k = 1,5.$$

This implies that $A_1^{(h)}$ and $A_{-1}^{(h)}$ are zero. The δ^4 part of Eq. (A8) gives

$$t_k A_1^{(4)} + t_k^{-1} A_{-1}^{(4)} + t_k^5 A_5^{(4)} + t_k^{-5} A_{-5}^{(4)} = 0, \quad \text{for} \quad k = 1,5.$$

These equations have two linearly independent solutions one of which satisfies Eq. (A2). Substituting these results into Eqs. (A7) and (A1) yields

$$g(\hat{z}) = t + t^{-1} + C(t^{-5} - t) + C^*(t^5 - t^{-1}) + O(\delta^5), \tag{A9}$$

where we have written

$$A_{-5}^{(4)}\delta^4 = C \quad \text{and} \quad A_5^{(4)}\delta^4 = C^*.$$

Note that Eq. (A9) can be written in the form (53). We have used Eqs. (A5) and (A6) only to come up with the series expansion (A7). These equations would be needed if the coefficients $A_p^{(h)}$ with $h > 4$ were to be determined. Knowledge of these coefficients would yield a solution to the integral equations (48) and (49) also for a finite opening between $\hat{b}_L$ and $\hat{b}_R$. Unfortunately we have not been able to calculate these coefficients, but fortunately they are not needed because the present purpose is only to compute ρ_L, ρ_R, ϕ_L, ϕ_R, and $\Phi = -(\Sigma_L + \Sigma_R)$ to leading order in δ.

As our aim is to calculate the quantities ρ_L, ρ_R, ϕ_L, ϕ_R, and Φ, we substitute Eqs. (A1) and (A7) into the integral expressions from Sec. VI A. For Eq. (57) this gives, after transforming to t as integration variable,

$$\rho_L = \frac{1}{2\pi i} \sum_{p=-\infty}^{\infty} \sum_{h=|p|-1}^{\infty} A_p^{(h)} \delta^h \int_{\beta_L \delta^{-1}}^{\beta_L \delta} t^p \frac{1}{\sqrt{\hat{z}^2 + 4}} \frac{d\hat{z}}{dt} dt. \tag{A10}$$

For each p and h we determine the order in δ of the contribution. When $t \to 0$ or $t \to \infty$, the integrand is proportional to t^{p+5} and t^{p-7}, respectively. Hence the integral is bounded, of order 0 in δ, that is, for $|p| \leqslant 5$, logarithmic in δ for $|p| = 6$, and of order $6 - |p|$ in δ for $|p| \geqslant 7$. Note that the coefficients $A_p^{(h)}$ with $|p| = 6$ are zero. Let m denote the order in δ of the integral. The order in δ of the whole contribution is $h + m$,

$\lvert p\rvert$	m	h	$h+m$
1	0	0	0
1	0	4	4
1	0	$\geqslant 5$	$\geqslant 5$
5	0	4	4
5	0	$\geqslant 5$	$\geqslant 5$
$\geqslant 7$	$6 - \lvert p\rvert$	$\geqslant \lvert p\rvert - 1$	$\geqslant 5$

Therefore ρ_L in Eq. (A10) has a δ^0 contribution from the unperturbed part in the RHS of Eq. (A9), a δ^4 contribution from the part involving C and C^*, and contributions of higher order in δ from the parts collected in the $O(\delta^5)$ term, so

$$\rho_L = \frac{1}{2\pi i} \int_{\beta_L \delta^{-1}}^{\beta_L \delta} [t + t^{-1} + C(t^{-5} - t) + C^*(t^5 - t^{-1})] \frac{1}{\sqrt{\hat{z}^2 + 4}} \frac{d\hat{z}}{dt} dt + O(\delta^5).$$

In the RHS the integration limits may be changed from $\beta_L \delta^{-1}$ and $\beta_L \delta$ to ∞ and 0 as this makes a difference $O(\delta^5)$. Transforming back to z as integration variable then gives

$$\rho_L = \frac{1}{2\pi i} \int_{\Xi^{(0)}} [t + t^{-1} + C(t^{-5} - t) + C^*(t^5 - t^{-1})] dz + O(\delta^5),$$

where $\Xi^{(0)}$ denotes the unperturbed ($\delta = 0$) contour. Hence ρ_L is given to leading order in $C \sim \delta^4$ by Eq. (57) where now $f(z)$ is given by Eq. (60) instead of Eq. (56), and integration is over the unperturbed contour. Note that β_L and β_R do not occur in this expression. Similar arguments show that fully analogous results hold for ρ_R, ϕ_L, ϕ_R, Σ_L, and Σ_R: Up to $O(\delta^5)$ they are given by the integrals (57), (58), and (59) or their R analogs, with $f(z)$ given by Eq. (60). Therefore we have now obtained these quantities to leading order, namely δ^4, in the parameter δ that describes the infinitesimally small opening $\hat{b}_L - \hat{b}_R \sim \delta^6$ between the end points of $\hat{\Xi}$ and $\hat{H}$.

[1] R. H. Fowler and G. S. Rushbrooke, Trans. Faraday Soc. **33**, 1272 (1937).
[2] P. W. Kasteleyn, Physica (Amsterdam) **27**, 1209 (1961).
[3] H. N. V. Temperley and M. E. Fisher, Philos. Mag. **6**, 1061 (1961).
[4] E. H. Lieb, Phys. Rev. Lett. **18**, 692 (1967).
[5] E. H. Lieb, Phys. Rev. **162**, 162 (1967).
[6] E. H. Lieb, Phys. Rev. Lett. **18**, 1046 (1967).
[7] E. H. Lieb, Phys. Rev. Lett. **19**, 108 (1967).
[8] B. Sutherland, Phys. Rev. Lett. **19**, 103 (1967).
[9] C. P. Yang, Phys. Rev. Lett. **19**, 586 (1967).
[10] B. Sutherland, C. N. Yang, and C. P. Yang, Phys. Rev. Lett. **19**, 588 (1967).
[11] E. H. Lieb and F. Y. Wu, in *Phase Transitions and Critical Phenomena*, edited by C. Domb and M. S. Green (Academic, London, 1972), Vol. 1, pp. 321–490.
[12] J. F. Nagle, C. S. O. Yokoi, and S. M. Bhattacharjee, in *Phase Transitions and Critical Phenomena*, edited by C. Domb and J. L. Lebowitz (Academic, London, 1989), Vol. 13, pp. 235–297.
[13] J. Villain, in *Ordering in Strongly Fluctuating Condensed Matter Systems*, edited by T. Riste (Plenum, New York, 1980), pp. 221–253.
[14] H. Kawamura, Prog. Theor. Phys. **70**, 352 (1983).
[15] M. Widom, Phys. Rev. Lett. **70**, 2094 (1993).
[16] P. A. Kalugin, J. Phys. A **27**, 3599 (1994).
[17] A. Verberkmoes and B. Nienhuis, Phys. Rev. Lett. **83**, 3986 (1999).
[18] J. de Gier and B. Nienhuis, J. Stat. Phys. **87**, 415 (1997).
[19] J. de Gier and B. Nienhuis, J. Phys. A **31**, 2141 (1998).
[20] R. J. Baxter, J. Math. Phys. **11**, 784 (1970).
[21] F. Y. Wu, Rev. Mod. Phys. **54**, 235 (1982).
[22] D. A. Huse and A. D. Rutenberg, Phys. Rev. B **45**, 7536 (1992).
[23] V. V. Bazhanov, Phys. Lett. **159B**, 321 (1985).
[24] M. Jimbo, Commun. Math. Phys. **102**, 537 (1986).
[25] R. J. Baxter, Ann. Phys. (N.Y.) **70**, 193 (1972).
[26] R. J. Baxter, *Exactly Solved Models in Statistical Mechanics* (Academic, London, 1982).
[27] L. D. Faddeev and L. A. Takhtadzhyan, J. Sov. Math. **24**, 241 (1984).
[28] N. Y. Reshetikhin, J. Phys. A **24**, 2387 (1991).
[29] J. de Gier and B. Nienhuis, Phys. Rev. E **55**, 3926 (1997).